AFRL-RX-WP-TR-2014-0162

AMERICA MAKES: NATIONAL ADDITIVE MANUFACTURING INNOVATION INSTITUTE (NAMII)
Project 1: Nondestructive Evaluation (NDE) of Complex Metallic Additive Manufactured (AM) Structures

Evgueni Todorov, Roger Spencer, Sean Gleeson, Madhi Jamshidinia, and Shawn M. Kelly

EWI

JUNE 2014
Interim Report

AIR FORCE RESEARCH LABORATORY
MATERIALS AND MANUFACTURING DIRECTORATE
WRIGHT-PATTERSON AIR FORCE BASE, OH 45433-7750
AIR FORCE MATERIEL COMMAND
UNITED STATES AIR FORCE

NOTICE AND SIGNATURE PAGE

____//SIGNATURE//_____   _____//SIGNATURE//_____

JOHN J. KLEEK   HOWARD S. SIZEK
Project Engineer   Branch Chief
Propulsion, Structures & Mfg Enterprise Branch   Propulsion, Structures & Mfg Enterprise Branch
Manufacturing & Industrial Technologies Div.   Manufacturing & Industrial Technologies Div.

REPORT DOCUMENTATION PAGE

Form Approved
OMB No. 0704-0188

The public reporting burden for this collection of information is estimated to average 1 hour per response, including the time for reviewing instructions, searching existing data sources, searching existing data sources, gathering and maintaining the data needed, and completing and reviewing the collection of information. Send comments regarding this burden estimate or any other aspect of this collection of information, including suggestions for reducing this burden, to Department of Defense, Washington Headquarters Services, Directorate for Information Operations and Reports (0704-0188), 1215 Jefferson Davis Highway, Suite 1204, Arlington, VA 22202-4302. Respondents should be aware that notwithstanding any other provision of law, no person shall be subject to any penalty for failing to comply with a collection of information if it does not display a currently valid OMB control number. **PLEASE DO NOT RETURN YOUR FORM TO THE ABOVE ADDRESS**.

1. REPORT DATE *(DD-MM-YY)* June 2014	2. REPORT TYPE Interim	3. DATES COVERED *(From - To)* 2 January 2014 – 30 May 2014	
4. TITLE AND SUBTITLE AMERICA MAKES: NATIONAL ADDITIVE MANUFACTURING INNOVATION INSTITUTE (NAMII) Project 1: Nondestructive Evaluation (NDE) of Complex Metallic Additive Manufactured (AM) Structures		**5a. CONTRACT NUMBER** FA8650-12-2-7230	
		5b. GRANT NUMBER	
		5c. PROGRAM ELEMENT NUMBER 63680F	
6. AUTHOR(S) Evgueni Todorov, Roger Spencer, Sean Gleeson, Madhi Jamshidinia, and Shawn M. Kelly		**5d. PROJECT NUMBER** 5280	
		5e. TASK NUMBER 00	
		5f. WORK UNIT NUMBER X0K4	
7. PERFORMING ORGANIZATION NAME(S) AND ADDRESS(ES) EWI 1250 Arthur E. Adams Drive Columbus, Ohio 43221		**8. PERFORMING ORGANIZATION REPORT NUMBER** 55028GTH	
9. SPONSORING/MONITORING AGENCY NAME(S) AND ADDRESS(ES) Air Force Research Laboratory Materials and Manufacturing Directorate Wright-Patterson Air Force Base, OH 45433-7750 Air Force Materiel Command United States Air Force		**10. SPONSORING/MONITORING AGENCY ACRONYM(S)** AFRL/RXMS	
		11. SPONSORING/MONITORING AGENCY REPORT NUMBER(S) AFRL-RX-WP-TR-2014-0162	

12. DISTRIBUTION/AVAILABILITY STATEMENT
Distribution Statement A: Approved for Public Release; Distribution is unlimited.

13. SUPPLEMENTARY NOTES
PA Case Number 88ABW-2014-4681; Clearance Date: 3 Oct 2014.. Report contains color.

14. ABSTRACT

Additive manufacturing (AM) has several advantages when applied to complex metallic components, particularly in the fabrication of low-volume, high-value parts. This study summarizes possible methods for performing nondestructive evaluation (NDE) of complex additively manufactured titanium and nickel based alloy components. In this report, a brief review of AM technologies is presented. Laser-Powder Bed Fusion (L-PBF) and Electron Beam Powder Bed Fusion (EB-PBF) are discussed in more detail as the two promising candidates for the production of components applicable in aerospace industry. Defect formation mechanisms and mitigation techniques are also discussed. Design complexity was qualitatively defined, and organized into 5 groups. A literature review was conducted to determine the industrial NDE techniques with the highest near (less than 3 years) and mid-term (3-5 years) potential to inspect titanium and nickel aerospace components produced by PBF processes. X-Ray Computed Tomography (X-ray CT) was selected as the most promising technique for complex geometries.

15. SUBJECT TERMS
additive manufacturing, selective laser melting, electron beam melting, non destructive evaluation (NDE)

16. SECURITY CLASSIFICATION OF:			17. LIMITATION OF ABSTRACT:	18. NUMBER OF PAGES	19a. NAME OF RESPONSIBLE PERSON (Monitor) John Kleek
a. REPORT Unclassified	**b. ABSTRACT** Unclassified	**c. THIS PAGE** Unclassified	SAR	70	19b. TELEPHONE NUMBER *(Include Area Code)* (937) 904-4894

Standard Form 298 (Rev. 8-98)
Prescribed by ANSI Std. Z39-18

ACKNOWLEDGEMENT

DISCLAIMER

TABLE OF CONTENTS

LIST OF FIGURES

LIST OF FIGURES

LIST OF TABLES

1.0   SUMMARY

Additive manufacturing (AM) has several advantages when applied to complex metallic components, particularly in the fabrication of low-volume, high-value parts. Capitalizing on the advantages of AM can allow performance enhancements, weight reduction, cost reduction, and decrease production time of the parent product. This study summarizes possible methods for performing nondestructive evaluation (NDE) of complex additively manufactured components. This research focused on Laser-Powder Bed Fusion (L-PBF) using titanium and nickel-based alloys.

In this report, a brief review of AM technologies is presented. L-PBF and Electron Beam Powder Bed Fusion (EB-PBF) are discussed in more detail, as the two promising candidates for the production of components applicable in aerospace industry. Defect formation mechanisms and mitigation techniques are also discussed.

Many industries can benefit from the advantages of AM technology; however, quality control issues must be adequately addressed prior to more widespread utilization. One of the key challenges is non-destructive inspection of AM fabricated components. While NDE techniques are well-developed, their application for inspection of AM components has not been fully established.

To determine applicable techniques for the NDE testing of AM components, design complexity was qualitatively defined, and organized into five groups. Components in Group 1 have the minimum design complexity and can be inspected using common NDE methods. Components in Group 5 have a high level of complexity, making their production by non-AM techniques impractical. New or creative application of existing NDE technologies is required for the inspection of this group.

A literature review was conducted to determine the industrial NDE techniques with the highest near (less than 3 years) and mid-term (3-5 years) potential to inspect titanium and nickel aerospace components produced by Powder Bed Fusion (PBF) processes. Down-selection criteria included the dependence of PBF process parameters on defect size, anisotropy in microstructure, material properties, component complexity, and the limitations of current NDE methods. Based on these criteria, X-Ray Computed Tomography (X-ray CT) was selected as the most promising NDE technique for the reliable inspection and characterization of complex geometries in Group 4 and 5 AM components.

The limited number of studies which address the utilization of NDE techniques for the inspection of AM components suggests a technical gap. As a result, performance of NDE techniques cannot be reliably predicted. Further, the challenges presented by the most complex AM components are not yet understood, resulting in an additional technical gap. The methodology required to address these technical gaps is discussed.

2.0 INTRODUCTION

Additive Manufacturing (AM) has several advantages when applied to the fabrication of complex metallic components, including:

- Single piece fabrication of complex components

- Fabrication of part geometries that would normally be too complicated, expensive, or impossible to fabricate using traditional subtractive techniques

- Reduced need for castings or forgings

- Addition of part complexity with minimal additional expense

- Direct fabrication of parts

These capabilities are advantageous when fabricating low-volume, high-value parts. AM allows performance enhancements, weight reduction, cost reduction, and decreased production time of the parent product.

For components that are fabricated under rigorous quality control programs in industries such as aerospace or nuclear, a part must comply with a certification process before it can be put into service. This process contains three primary components: fabrication, process control, and validation/quality control (Figure 1). When considering this certification cycle for AM parts, the fabrication and process control steps are relatively well known, but the validation/quality control step has yet to be fully established. Considering the broad discipline of quality control, one of the key features is the ability to inspect the fabricated components nondestructively after they have been produced to verify that the part does not contain volumetric discontinuities, surface-breaking discontinuities, or other unacceptable conditions.

```
┌─────────────┐     ┌──────────────┐     ┌──────────────────┐     ┌──────────────┐
│ Design Part │ ──▶ │ Fabricate with│ ──▶ │ Inspect / Validate for│ ──▶ │ Implement Part│
│             │     │ Process under │     │ Quality Assurance │     │  in Service  │
│             │     │   Control    │     │  and Airworthiness│     │              │
└─────────────┘     └──────────────┘     └──────────────────┘     └──────────────┘
```
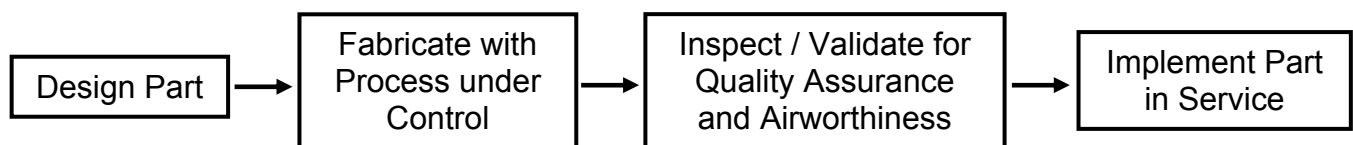
Figure 1. "Simplified" Component Certification Cycle

NDE techniques have been used successfully in quality control for decades. When NDE is applied to AM parts, the advantages of AM become the limiting factors in the ability to validate the part. These limiting factors consist of the following two categories:

- **Geometry**
  - Complexity
  - Thick to thin (density differences)
  - Embedded features
  - Thickness of the build layers
  - Organic part design

2

- **Material Properties**
  - Dissimilar metals
  - Surface finish
  - Ferrous/nonferrous
  - Residual stress
  - Microstructure non-uniformity and anisotropy

These inspection considerations are not unique to AM, in fact, they are considered in all NDE applications. Adding design complexity can have a dramatic effect on inspectability (Figure 2). Geometric complexity is a primary factor defining the ability to apply post-process inspection to AM parts. This report provides a brief overview of AM processes with typical defects and conditions. Next, the report describes a scaled definition of geometric complexity, from those parts that can be made using conventional manufacturing techniques, to those parts that can only be manufactured additively. A literature review provides examples of NDE applied to AM. While application of conventional NDE techniques is suitable for simple geometric components, more complex components require expansion to inspection techniques outside the typical toolbox available to NDE engineers. Examples of NDE techniques from medical industry have been included along with discussion on how they might be applied to the AM components with complex geometry.

The objectives of this project were to:

- Evaluate capabilities of existing NDE technique in terms of their applicability to AM components with complex geometry.

- Down-select NDE techniques that might be possible to optimize and validate for post process NDE of AM components.
- Provide recommendations for future work.
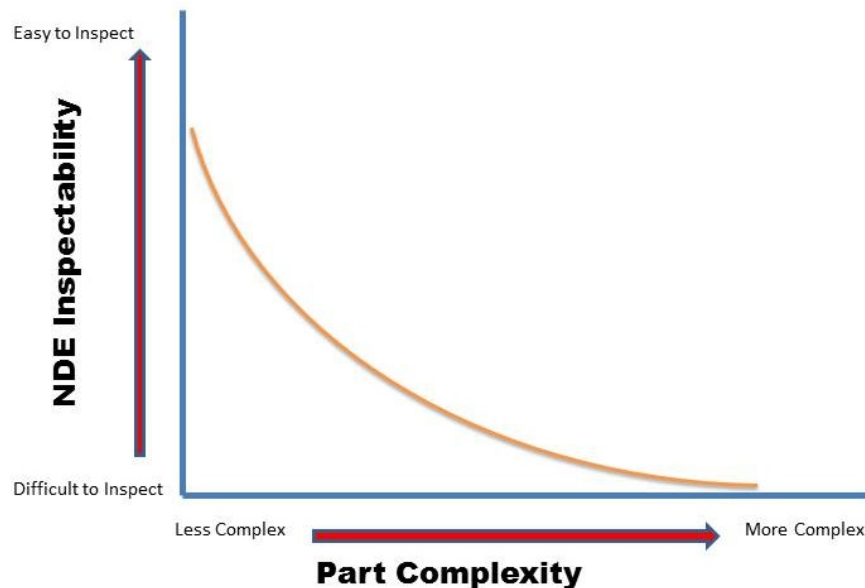
Figure 2. Complexity vs. Inspectability

3

3.0 METHODS, ASSUMPTIONS AND PROCEDURES

A literature review was conducted to determine the applicability of various NDE techniques for post process NDE examination of AM components. Assumptions regarding the capabilities of existing NDE techniques were made after analyzing various AM processes, typical defects and conditions, geometric complexity ranking, past experience, and published data on NDE performance when inspecting conventional wrought products and AM components.

4.0 RESULTS

The literature search was focused on existing conventional and advanced NDE techniques that could inspect AM parts and components made of titanium and nickel-base alloys after AM fabrication.

4.1 Additive Manufacturing Methods and Applications

Three-dimensional printing (3D Printing) and AM are two terms that have been used interchangeably over recent years. These technologies are also known by such names as freeform fabrication, solid freeform fabrication, rapid prototyping, and rapid manufacturing.[1] Flexibility, higher production speed, and cost effectiveness of these processes make them an attractive solution for individual or personalized demands.[2] Gibson, et al. define AM as a range of technologies that are capable of translating virtual solid model data into physical models, in a layer-by-layer manner.[3] It can be argued that Gibson's definition of AM is defining the process of 3D printing, while additive manufacturing considers the broad application of 3D printing, and necessary manufacturing steps to support its use in a production setting, such as nondestructive inspection.

In 2013, McKinsey Global Institute estimated that 3D printing could generate an economic impact of $230 billion to $550 billion per year by 2025.[4] According to the 2014 Wohlers Report, the 3D printing market grew to $3.07 billion in 2013. A compound annual growth rate of 34.9% was recorded as the highest in 17 years. Over the past 26 years, worldwide revenue has had an average growth of 27%.[4] These metrics indicate that the field continues to grow. Gibson, Wohlers, Guo and Bourell provide more detailed information on the background, state-of-the-industry, and future trend of additive manufacturing technology. [1,3,5,8]

4.1.1 Additive Manufacturing Methods and Materials

There are additive manufacturing processes for metals, polymers, and ceramics. In all additive manufacturing processes, a three-dimensional (3D) component is built layer by layer using some combination of an energy source and material feedstock. Energy sources range from resistive heaters to electron beams, and feedstock exist as uncured resins to metallic powder particles. The interaction of the energy source and feedstock, coupled with manipulation according to an interpretation of a solid model, produces a layer. Multiple layers added together yield a 3D component.

Slattery et al.[6] described how the general procedure followed in any AM process could be divided into the following eight steps, as presented in Figure 3.

(1) Prepare the computer-aided design (CAD) of the desired part

(2) Convert the CAD file to the stereo lithography (STL) file format and correct errors

(3) Transfer the sliced version of STL file to the 3D printing machine

(4) Set up the parameters related to the machine, heat source and material

(5) Build the part

(6) Remove the part

5

(7) Perform the desired post-processing steps such as cleaning, support removal, heat treatment, and post process inspection

(8) Application of the part as a functional component

Figure 4 presents the information regarding the most common additive manufacturing techniques, according to Wong et al.[7] and Gue and Leo summarized the types of materials that can be processed by AM technology (Table 1).[8] The remainder of this report discusses techniques to manufacture complex metallic components of interest to the aerospace community using AM. The specific AM technique is known as powder bed fusion (PBF) which uses thermal energy to selectively fuse regions of a powder bed.[9] Commercially available PBF systems for producing metal components employ laser (L-PBF) or electron beam (EB-PBF) energy sources. L-PBF and EB-PBF are capable of producing complex metallic components that take full advantage of the capabilities of additive manufacturing.

1 CAD
2 STL convert
3 File transfer to machine
4 Machine setup
5 Build
6 Remove
7 Post-process
8 Application
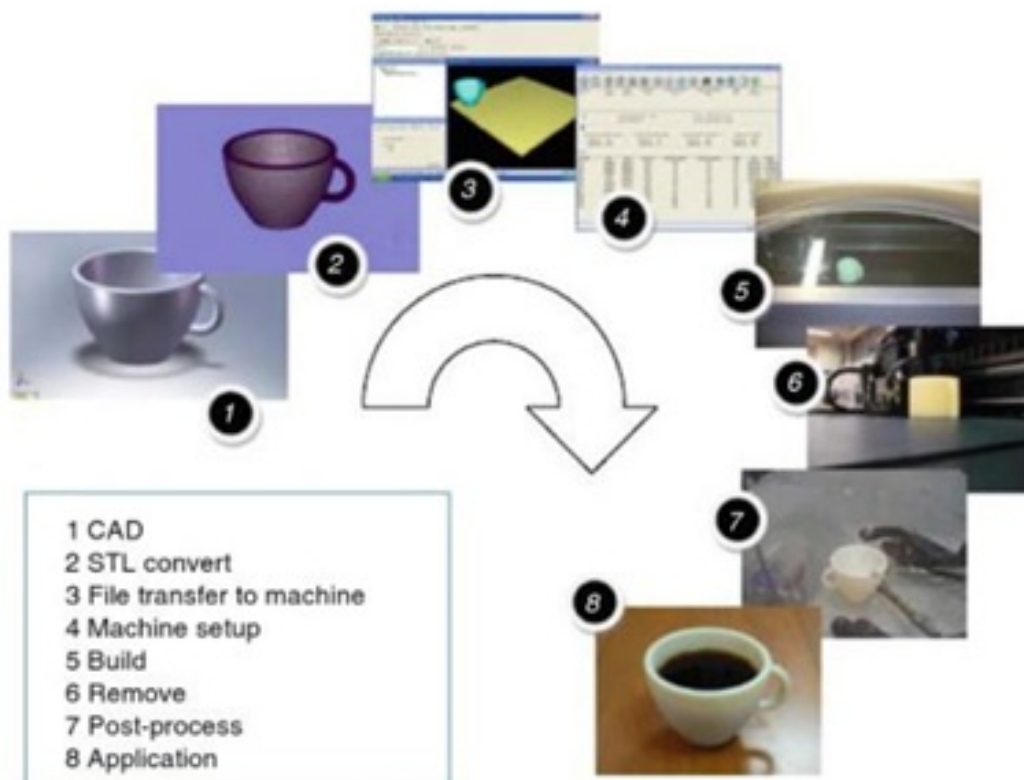
Figure 3. General 8 Steps for Any Additive Manufacturing Process [10]
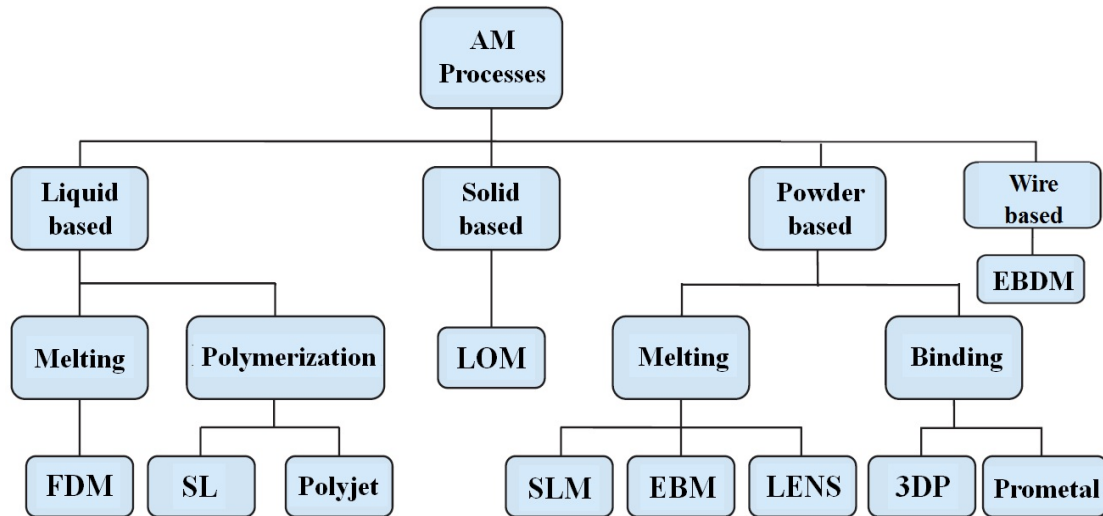
Figure 4. Additive Manufacturing Technologies

4.1.2 Powder Bed Fusion (PBF) Processes

Among the processes shown in Figure 4, SLM™ (SLM Solutions, Germany), EBM™ (Arcam, Sweden), LENS™(Optomec, Albuquerque, NM), and EBDM™(Sciaky, Chicago, IL) are processes that are appropriately developed for additive manufacturing of metals. The two powder bed fusion processes are SLM and EBM, while LENS and EBDM are directed energy deposition processes. Powder bed fusion processes are capable of producing more complicated geometries, which present the greatest challenge for post process inspection. Among the laser based powder bed fusion (L-PBF) processes there are several commercially available systems (Direct Metal Laser Sintering™ (EOS, Germany), Selective Laser Melting™ (SLM Solutions, Germany), LaserCUSING™ (Concept Laser, Germany), LaserMelting (Renishaw, UK), Phenix (3D Systems, Rock Hill, NC)). EBM is the only commercially available EB-PBF system. The following provides a brief description of the fundamentals of two mentioned technologies.

Table 1.   Materials and Corresponding AM Processes [8]

Material type		AM process(es)	Manufacturer/research institute(s)	Material(s)
Polymers[a]	Thermo-setting	SLA, MJM	3D Systems	Photo-curable polymers
	Thermo-plastic	MJM	3D Systems	Wax
		SLS	EOS	Polyamide 12, GF polyamide, polystyrene
		FDM	Stratasys	ABS, PC-ABS, PC, ULTEM
		3DP	3D Systems	Acrylic plastics, wax
Metals[a]		SLM	EOS	Stainless steel GP1, PH1 and 17-4, cobalt chrome MP1, titanium Ti6Al4V, Ti6Al4V ELI and TiCP, IN718, maraging steel MS1, AlSi20Mg
		LDM/LENS	Optomec	Steel H13, 17-4 PH, PH 13-8 Mo, 304, 316 and 420, aluminum 4047, titanium TiCP, Ti-6-4, Ti-6-2-4-2 and Ti6-2-4-6, IN625, IN617, Cu-Ni alloy, cobalt satellite 21
		EBM	Arcam	Ti6Al4V, Ti6Al4V ELI, cobalt chrome
Ceramics[b]		SLA	[76–78]	Suspension of Zirconia, silica, alumina, or other ceramic particles in liquid resin
		FDM	[79–81]	Alumina, PZT, Si_3N_4, zirconia, silica, bioceramic
		SLS	[82–85]	Alumina, silica, zirconia, ZrB_2, bioceramic, graphite, bioglass, and various sands
		3DP	[64,86]	Zirconia, silica, alumina, Ti3SiC2, bioceramic, and various sands
Composites[b]	Uniform composites	FDM	[87–89]	Polymer-metal, polymer-ceramic, short fiber-reinforced composites
		3DP	[90,91]	Polymer-matrix, metal-ceramic, ceramic-ceramic short fiber-reinforced composites
		LOM	[92–94]	Polymer-matrix, ceramic-matrix, fiber and particulate-reinforced composites
		SLS, SLM	[95–100]	Metal-metal, metal-ceramic, ceramic-ceramic, polymer-matrix, short fiber-reinforced composites
	FGM	LMD/LENS	[57,101–105]	CoCrMo/Ti6Al4V, TiC/Ti, Ti/TiO$_2$, Ti6Al4V/IN718
		FDM	[30]	PZT
		FEF	[106]	Al_2O_3/ZrO_2

Notes: a) Commercially available materials for AM processes; b) materials under research and development

4.1.2.1 Laser Powder Bed Fusion (L-PBF) Processes

Bineli et. al. describes the L-PBF process for Direct Metal Laser Sintering equipment shown in Figure 5.[10] In the L-PBF process, part fabrication takes place in an inert atmosphere that depends on the equipment and material being produced. The build platform (i.e., building plate, or substrate) is preheated to a temperature that is generally below 100°C. A recoating system spreads a thin layer of powder (stored in the dispenser) over the build platform. This layer-thickness of powder can range from 20 to 80 μm, depending on the machine and material. The thickness of the powder layer is adjusted by the appropriate movement of dispenser and building platforms along the building direction. Excess metal powder falls into the collector for re-use. Next a laser beam is scanned over the powder bed according to a tool path that is generated from the 3D model of the part. Lasers used in current L-PBF processes are solid state with a nominal wavelength of 1 μm, and are operated in continuous wave mode. Power outputs range from 200 W to up 1000 W of maximum continuous power output. The absorption of laser energy melts the metal powder, resulting in the formation of a metallurgical bond between the current and pre-deposited layers. This process proceeds until the whole 3D design is manufactured.
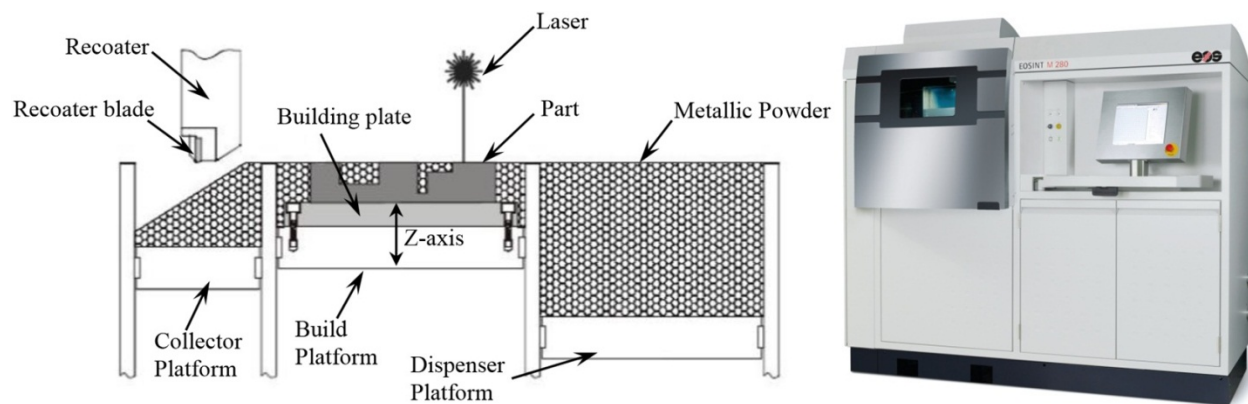
Figure 5.   Schematic of Laser Powder-Bed Fusion (L-PBF) Process (left)**;
EOSINT M280 Machine** (right)

4.1.2.2 Electron Beam Powder Bed Fusion (EB-PBF) Processes

Jamshidinia et al.[11] draw a schematic of the EB-PBF process, shown in Figure 6. In the first step, a 3D CAD model stored in a STL format is used as an input into the buildup file for the EB-PBF machine. Electrons are produced by heating the tungsten filament, and then accelerated by applying a high voltage between the anode and cathode. In the next step, electrons pass through three coils which are used to focus and steer the beam. Upon striking the target material, the kinetic energy of electrons is transformed into heat. The generated heat is used for preheating the substrate (stainless steel plate). When the desired preheating temperature is reached, the powder rake applies the first powder layer. According to the uploaded 3D CAD design, the electron beam scans the powder bed and fully melts the powder where a solid is needed. The rest of the powder is scanned by a lower power and partially melts, where solid is not needed. The partially sintered powder acts as a support (called volume support) for the over-hanged structures that will be built in the next layers. After removing the part from the EB-PBF machine, the partially sintered powder is broken away in a powder recycling unit.[12]
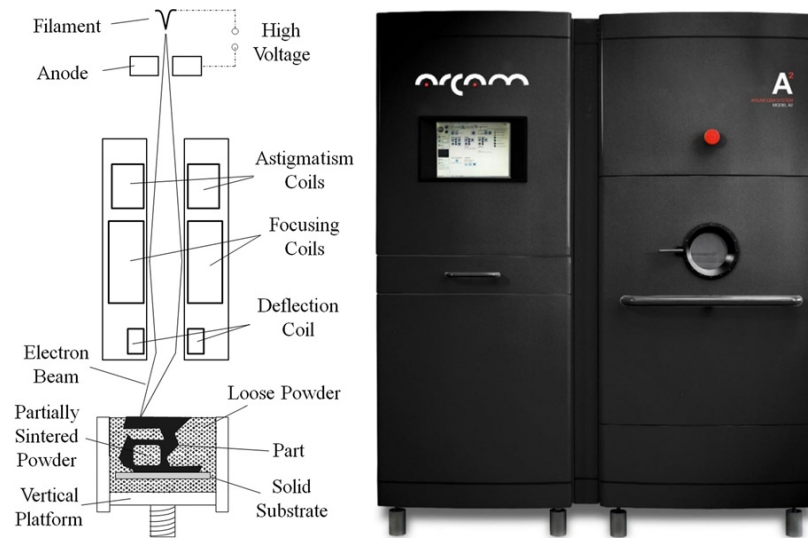
Figure 6. Schematic of Electron Beam Melting Machine Setup (left),[11] **ARCAM A2 Machine** (right) *(Courtesy of ARCAM AB, Sweden)*

4.1.2.3 Comparison of L-PBF and EB-PBF Processes

Gibson, et al. summarized the differences between L-PBF and EB-PBF, shown in Table 2.[3] The higher energy density and higher scanning speed in EB-PBF results in the superior build rate, compared to L-PBF. According to Guo and Leu, the surface finish and feature resolution in parts produced by L-PBF are much better than those produced by EB-PBF.[8] The tradeoff between surface finish/feature resolution and build rate is attributed to differences in the beam diameter and size of the metal powder employed. These differences are summarized in Table 3. Mahale showed that the preheating of the substrate in EB-PBF minimizes thermal gradient and consequently residual stress.[12] On the other hand, EB-PBF process has a limited number of standard available metallic materials, while L-PBF supports a much broader range of materials including metals, ceramics, and polymers.

Table 2. Comparison of EB-PBF (Electron Beam Melting) and L-PBF (Selective Laser Melting)[3]

Characteristic	Electron beam melting	Selective laser melting
Thermal source	Electron beam	Laser
Atmosphere	Vacuum	Inert gas
Scanning	Deflection coils	Galvanometers
Energy absorption	Conductivity-limited	Absorptivity-limited
Powder pre-heating	Use electron beam	Use infrared heaters
Scan speeds	Very fast, magnetically-driven	Limited by galvanometer inertia
Energy costs	Moderate	High
Surface finish	Moderate to poor	Excellent to moderate
Feature resolution	Moderate	Excellent
Materials	Metals (conductors)	Polymers, metals and ceramics

Table 3.   Typical Beam and Powder Size Ranges for PBF Processes

Process	Beam Size (µm)	Powder Size (µm)
L-PBF	100-150[13]	20-50[17]
EB-PBF	100-500[14,15] (50[16])	45-100[18](a)

(a) Several ranges of average size of powder particles have been reported in academic studies, such as 10-100 µm,[19] 10-60 µm,[20] and average size of 40 µm.[21] Therefore, the ARCAM company's website was used as the most reliable source.

4.1.3   Applications of Additive Manufacturing in Aerospace Industry

Bourell et. al. summarized the diverse applications of additive manufacturing technology in Figure 7.[22]   Virtually all industries have the ability to benefit in some way from AM, though early adopters of the technology fall in the aerospace and medical sectors. According to Huang and Leu, early adoption by the aerospace industry was driven by the remarkable benefits and applications of AM.[23] The complex geometries of components demanded in limited quantity as well as the advanced materials used in the aerospace industry make conventional methods of manufacturing costly and time consuming. AM has been shown to be suitable for aerospace applications by reducing material waste and manufacturing time, producing parts with optimized geometries, and providing on-demand manufacture and replacement. According to Antonysamy,[24] engine blades and vanes are examples of aerospace components with complex geometries that usually contain internal channels for cooling purposes. These components are mostly made of titanium or nickel-base alloys, and a lower buy-to-fly ratio contributed by AM can result in considerable savings in manufacturing costs. Figure 8 shows examples of components produced by powder-bed additive manufacturing processes for aerospace applications.

4.1.4   Powder Bed Fusion and Post Process Inspection

This section describes the types of defects that have been reported in the literature for PBF processes. They may result from inadequate process parameters, process controls, or the geometry of the parts produced. Attar introduced some of the most common defects produced during powder-bed additive manufacturing, such as porosity, lack of fusion, balling, surface roughness, and cracking due to solidification or residual stress.[25] These defects, which may result in degradation of part quality, are described in the following sections.

4.1.4.1   Volumetric Defects: Porosity and Lack of Fusion

Porosity and lack of fusion are two types of volumetric defects that may be created in L-PBF processes. Porosity is generally described as being spherical while lack of fusion can be irregular shaped and may contain unmelted powder particles. The formation of these defects may be driven by energy input being too high or too low, contamination, or other incorrectly established parameters. Gong et al. compared the effect of energy input (laser power and scanning speed) on porosity and lack of fusion in L-PBF Ti-6Al-4V.[26] Figure 9 shows that at a given power level, scanning at reduced scan speed leads to porosity formation, while scanning at a high speed can lead to lack of fusion discontinuities.
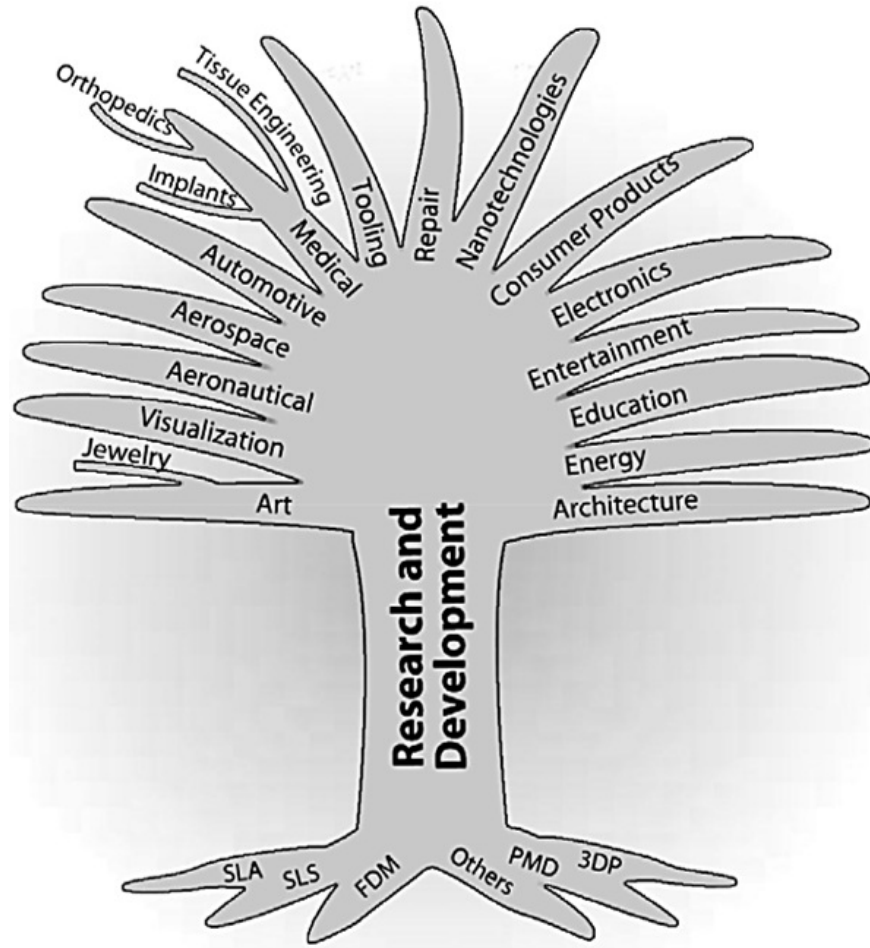
Figure 7. Schematic Visualization of AM Field and Research Opportunities and Effort[22]
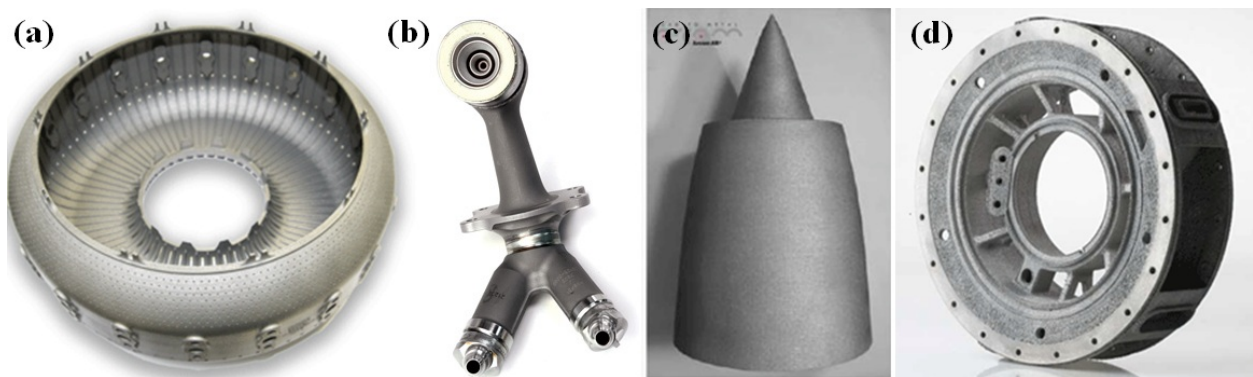
Figure 8.   Examples of Components Produced by Powder-Bed AM for Aerospace Application: (a) Combustion chamber made of IN 718 *(Courtesy EOS)***; (b) General Electric (GE) Leap Engine fuel nozzle made of Co-Cr alloy** *(Courtesy GE Aviation)***; (c, d) aerospace prototypes made of Ti-6Al-4V** *(Courtesy ARCAM AB, Sweden)*
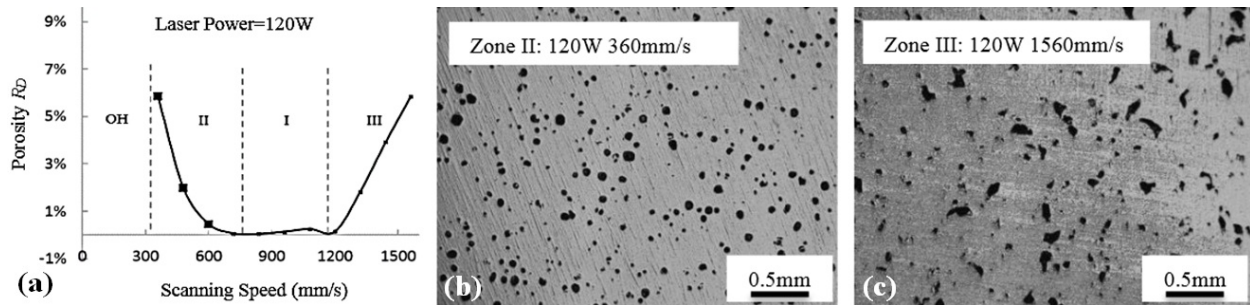
Figure 9. Formation of Porosity in Selective Laser Melting: (a) Influence of laser power and scanning speed on the type of defects; (b) Cross sectional view of coupon with defect caused by high energy input; and, (c) Cross sectional view of coupon with lack of fusion caused by low energy input[26]
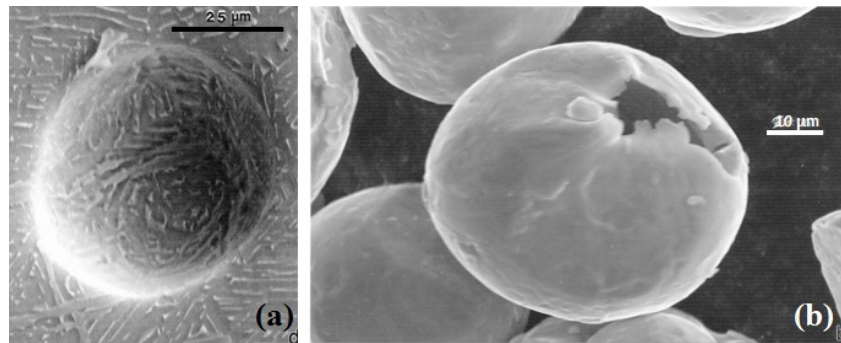
Figure 10. Formation of Porosity Caused by Powder Contamination: (a) Scanning Electron Microscope (SEM) image of gas bubble generated in structure of Ti-6Al-4V; and, (b) SEM image of gas bubble breaking powder particle[27]

Gaytan, et al. have shown another cause for porosity formation in metal PBF processes.[27] During the atomization process, argon might be trapped in Ti-6Al-4V particles. The trapped argon is carried into molten pool and results in the formation of gas bubbles (voids). Figure 10 shows the examples of porosity in Ti-6Al-4V specimens produced by EB-PBF. The application of post hot isostatic pressing (HIP) process can largely eliminate porosity. Also, it is reported by Gaytan et al. that the small size voids left in the structure may not impact the short-term mechanical properties of EB-PBF parts.[27]

4.1.4.2 Cracking and Delamination

Vrancken et al. stated the application of a high intensity (focused) beam and the fast cooling rate in the mentioned powder-bed additive manufacturing processes leads to the establishment of a large thermal gradient through a part.[28] The presence of thermal stress can result in delamination of a part from the substrate (Figure 11a) or cracking of the part (Figure 11b), especially in large components with higher levels of developed stresses. Also, residual stresses can influence the dimensional accuracy of a part. Any structure with low geometrical stiffness such as thin walls and overhang structures are more prone to deformation. In addition, the tensile residual stress formed on the surface of a part can reduce the effective structural load that can be applied on the part.[28]
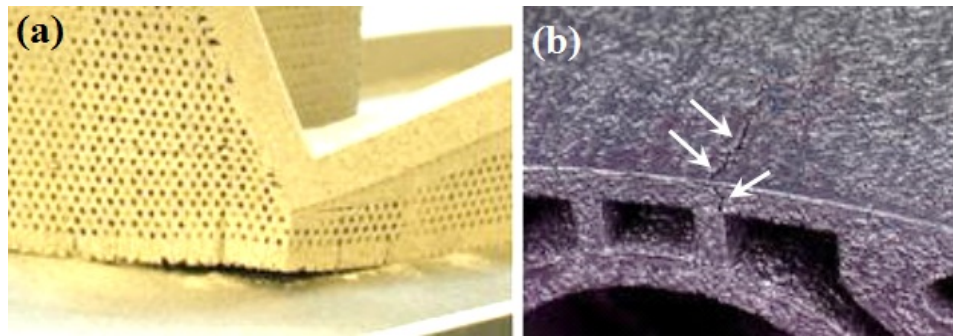
Figure 11. Defects Caused by Residual Stresses Developed during Selective Laser Melting: a) Delamination from Substrate; b) Cracking of Part; white arrows show crack[29]

4.1.4.3 Balling

According to Li et al.[30] and Gu and Shen[31] the application of high scanning speed, low laser power, increased thickness of powder layer or high level of oxygen might cause another issue known as the balling effect. Attar[25] defined the balling phenomenon as the formation of small spheres of solidified materials, with the approximate size of the beam diameter. In the mentioned cases, the surface tension of molten material exceeds the wettability of the pre-solidified layer, and the thin layer of molten pool breaks up into spherical droplets.[30, 31] Figure 12 shows the formation of balling during the L-PBF process.[31] Balling or other changes in the shape of individual tracks would result in the formation of volumetric defects, primarily lack of fusion in addition to poor surface finish.[25]

4.1.4.4 Surface Roughness

Surface roughness, while not explicitly a defect, is a characteristic of PBF processes that needs to be considered in the context of post process nondestructive inspection. Attar[25] schematically showed the influence of the stair-stepping effect on surface roughness in additive manufacturing (Figure 13). Since a CAD model is actually built by stacking consecutive layers upon each other, any non-horizontal and non-upward facing surface tends to be rough. A decrease in the thickness of powder layer lowers the stair-stepping effect.[25] The same effect on the surface roughness is reported by using a finer powder size.[25] Also, bimodal powder size distribution can improve the powder packing and decrease surface roughness.[25] In addition, process parameters can considerably influence surface roughness. Safdar et al.[32] concluded that an increase in beam current, or a decrease in offset focus and scanning speed, can result in the formation of a larger molten pool, and consequently, a higher surface roughness. Size and design of a component,[32] and even the arrangement of components inside the chamber, can change the amount of heat accumulated between them and change surface roughness, according to Jamshidinia and Kovacevic.[33] Das[34] and Agarwala et al.[35] studied the influence of surface tension on surface roughness. It was shown that surface tension can affect the flow regime in the molten pool, and consequently surface roughness. Chemical composition, impurity, and temperature are among the parameters that can alter surface tension of a material.[34,35]
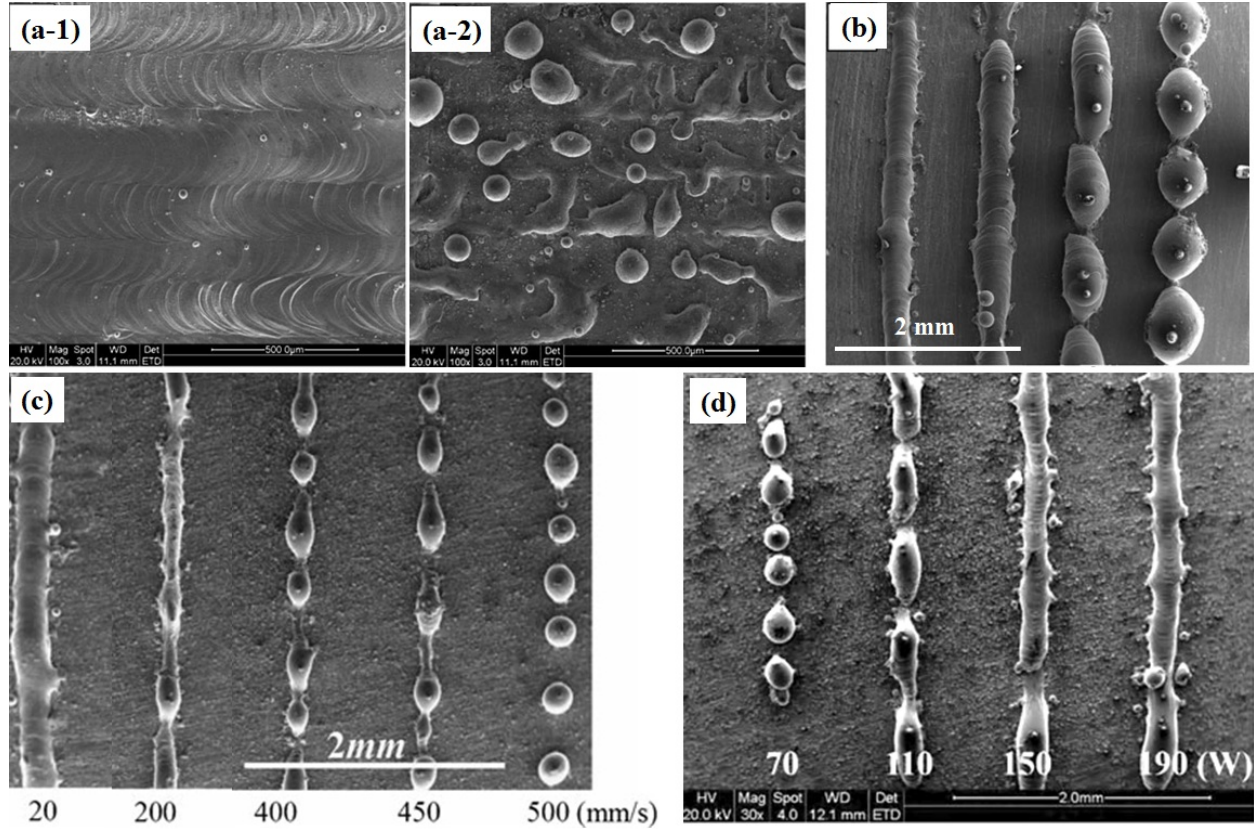
Figure 12. **Influence of Process Parameters on Occurrence of Balling during L-PBF: Increasing oxygen content in atmosphere (a-1) 0.1%, (a-2) 10%; (b) Thickness of powder layer, increasing from left to right; (c) Laser scanning speed, increasing from left to right; (d) Laser power, increasing from left to right[30]**
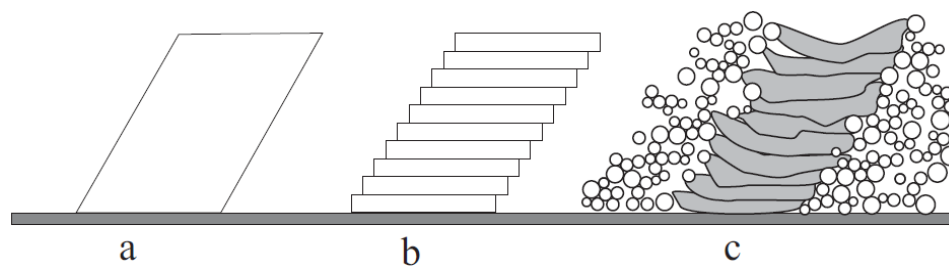
Figure 13. **Schematic of Influence of Stair-stepping Effect on Surface Roughness in Additive Manufacturing: (a) CAD data; (b) Slicing and resultant stair-stepping effect; (c) layer-by-layer manufactured wall with surface irregularity.[25]**

Several parameters can influence the surface roughness of a component produced by powder bed additive manufacturing techniques. Therefore, different ranges of surface roughness have been reported for both EB-PBF and L-PBF. However, because of the application of a higher intensity beam and scanning speed, larger powder particles, and thicker powder layer, EB-PBF produces rougher surfaces, compared to L-PBF. For example, Campanelli et al.[36] and Ponader et al.[37] reported two ranges of 6-14 μm and 24.9-96.7 μm for the L-PBF and EB-PBF of Ti-6Al-4V, respectively. Koike et al.[21] compared the surface roughness of the Ti-6Al-4V ELI tensile specimens, fabricated by L-PBF, EB-PBF, and casting (Figure 14). As shown, EB-PBF fabricated specimen has the highest surface roughness due to the coarser powder used.

(a) LBM Ti-6Al-4V ELI   (b) EBM Ti-6Al-4V ELI   (c) Cast Ti-6Al-4V ELI
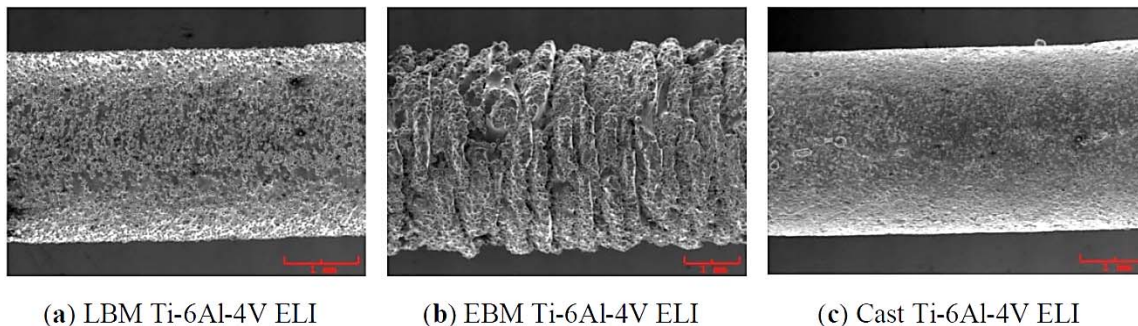
Figure 14.   Comparison of Surface Roughness of Cylinders Fabricated by (a) L-PBF (SLM); (b) EB-PBF (EBM); and (c) Casting[21]

4.1.5 Microstructural Issues

Microstructure can present challenges when using conventional nondestructive evaluation techniques. The layer-by-layer manufacturing of a component by using PBF processes is accompanied by the establishment of a unidirectional heat transfer along the build direction. Because grain growth during solidification preferably occurs in the opposite direction of heat transfer, the formation of elongated grains along the build direction is common, especially in alloys such as Ti-6Al-4V, and to a lesser extent, nickel alloy 718. For example, large grain size and anisotropy may result in increased attenuation and skewing of the acoustic beam when performing an ultrasonic examination. This issue is discussed more in detail in Section 4.3.1.8.

4.2 Additive Manufacturing Design Complexity Groupings

One of the advantages of additive manufacturing is design freedom, and the ability to produce shapes that cannot be produced using conventional manufacturing methods. With increasing complexity, the ability to conduct post-process inspection becomes increasingly difficult. One of the first steps in the literature study was to qualitatively define complexity in additive manufacturing to more clearly define the techniques to non-destructively inspect them. Complexity is difficult to quantitatively define and the subject matter is a broad topic. Kerbrat et al. define complexity as it influences manufacturing time, cost and quality using geometric parameters, material and technical specifications for developing a manufacturability index.[38] Such an index focuses on how complexity influences component manufacturability more than inspectability. As a result, a manufacturing index was not applicable to this study. Kroll et al. investigated AM and quality assurance during the part development process, providing some quality criteria without fully defining or segregating components by complexity.[39] It was determined that these complexity criteria were not completely relevant to this study.

For this study, a simple system for qualitatively grouping the range of complex metallic AM parts was developed. The approach categorizes components following an intuitive natural progression as one might discover and advance their skill level using AM. The grouping method will facilitate the discussion of possible strategies around how complexity affects the inspectability of a part or component. As this report investigates an NDE technique that is most applicable to AM components, it will include the group number or numbers to which that technique may apply.

4.2.1 Group 1: Simple Tools and Components

Generally, when an organization begins using AM it starts by producing basic parts that it already has the ability to fabricate (Figure 15). These items are generally simple in nature, but do not fully capitalize on the true advantages of AM. The components are well established and may already have NDE inspection procedures. These parts can be manufactured using basic subtractive manufacturing techniques applying one or two basic fabrication operations. Access to all surface features is unquestionably available on all Group 1 parts. It should be noted that in certain cases a Group 1 component may have been conventionally produced from a billet or forging of material that was nondestructively inspected prior to manufacturing. While AM eliminates these early inspection steps, the need for post AM inspection is required. Because of the simplicity of the part, superficial inspection is generally applicable, and any current NDE technology could provide acceptable results.
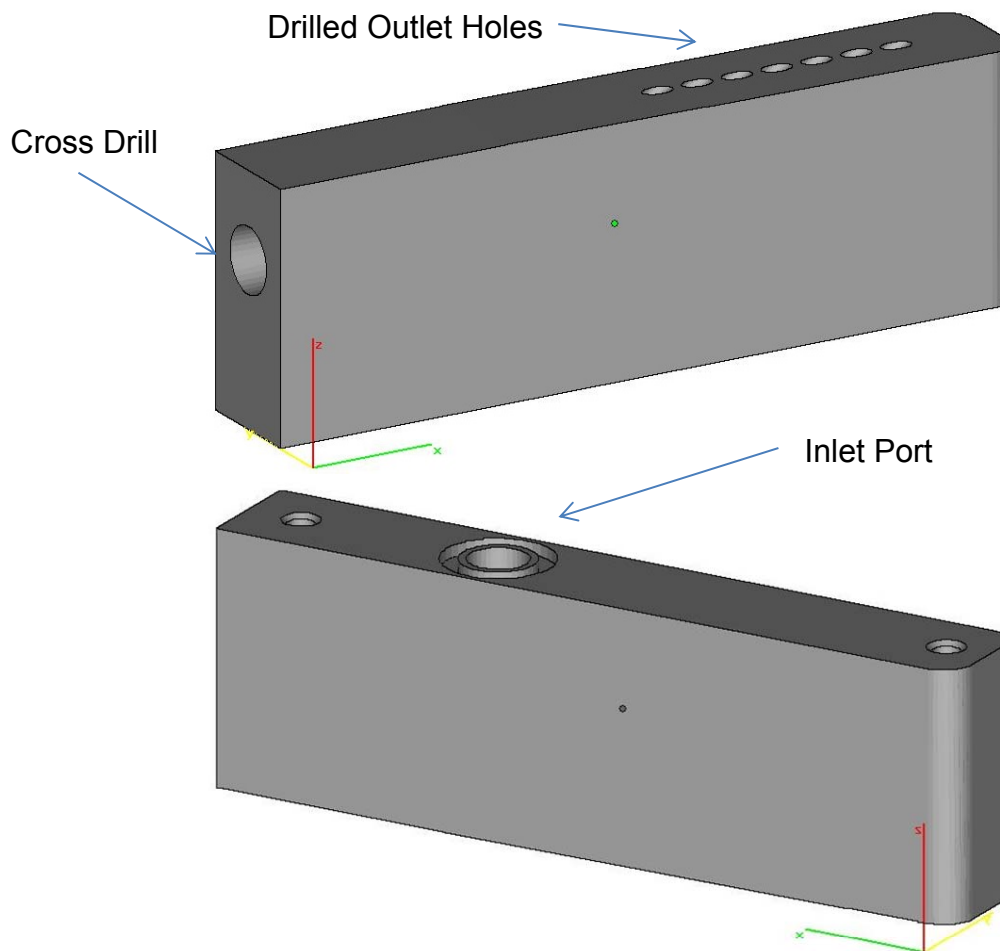
Figure 15.   Simple Subtractive Manufactured Component, Representative of Group 1

17

4.2.2　Group 2: Optimized Standard Parts

As a user progresses in their skill level and understanding of the capabilities of AM, they have a tendency to modify a part that they normally fabricate with traditional techniques, and to add features that they believe will increase its performance. Figure 16(a-b) shows an example of this progression. In 2013, GE Aviation launched a crowd source challenge to reduce the weight of a standard forged titanium engine mounting bracket (Figure 16a) by 30% while maintaining the level of performance.[40] Figure 16b shows the optimized design which resulted in an 84% reduction in weight and equivalent performance.

(a)   (b)
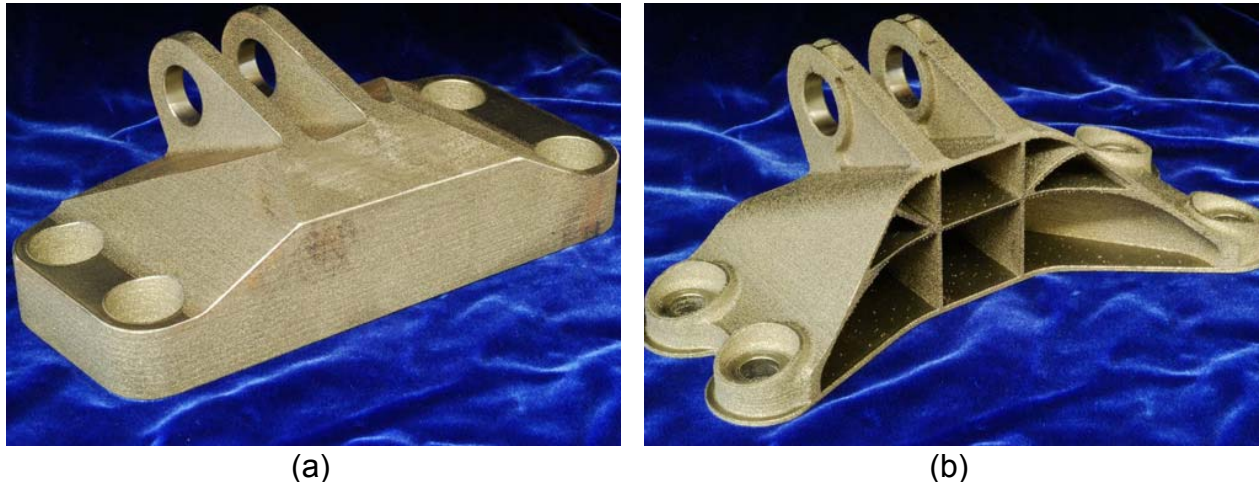
Figure 16.　**Titanium Alloy Aero-Engine Mounting Brackets Produced with L-PBF Representative of (a) Group 1 and (b) Group 2 Having Significantly Reduced Weight and Similar Mechanical Performance** *(Images from General Electric Corporation)*[40]

Prior to AM, incorporation of the added feature may have been too costly. These extra features start to add complexity to a part, thereby decreasing its inspectability. Parts that are normally fabricated using traditional methods, but have features added to enhance a particular characteristic, are considered AM Complexity Group 2. Subtractive fabrication of Group 2 parts require more complicated machining techniques and equipment. This type of part would not be easily fabricated using manually operated machine tools. They often require specialized tooling such as fluted or radius cutters along with multi-step operations and tool changes. Cost-effective manufacture of Group 2 components generally requires using Computer Numeric Control (CNC) equipment with automated tool changes and parameter settings. Clear "line of sight" to all features is available for tooling access, although the sequence of operations becomes important to the fabrication process on Group 2 parts. Spatial access to surfaces begins to narrow the NDE technology utilized, unless modified specifically for the part.

4.2.3　Group 3: Embedded Features

As the user continues to become more comfortable with the technology, it becomes apparent that they can include features such as internal tubing or channels. Internal components would normally cause the part to be fabricated using casting methods. Figure 17 shows an example of a Group 3 injection molding tool fabricated using L-PBF, where internal channels are directly produced in the part.[41] Parts that have their origin in a traditional part, then greatly modified to

include embedded features, are AM Complexity Group 3. These parts are not full "design for AM" because they are still a modification of an existing part. As a whole, Group 3 components cannot be manufactured using traditional subtractive fabrication techniques. The key to a Group 3 component is that traditional manufacture would require multiple machine components and an assembly phase. Additionally, when applying traditional subtractive manufacturing technology, the individual assembly components would, by and large, be considered Group 2 style fabrications. Therefore, the complexity of the individual part dictates the assembly requirement, and not some cost savings or material conservation criteria.

These AM parts contain features with no clear "line of sight" for tooling access. The embedded features can greatly add to the complexity of the part, thereby reducing the inspectability and the applicable NDE methods to those techniques that can image interior features.

(a) (b)
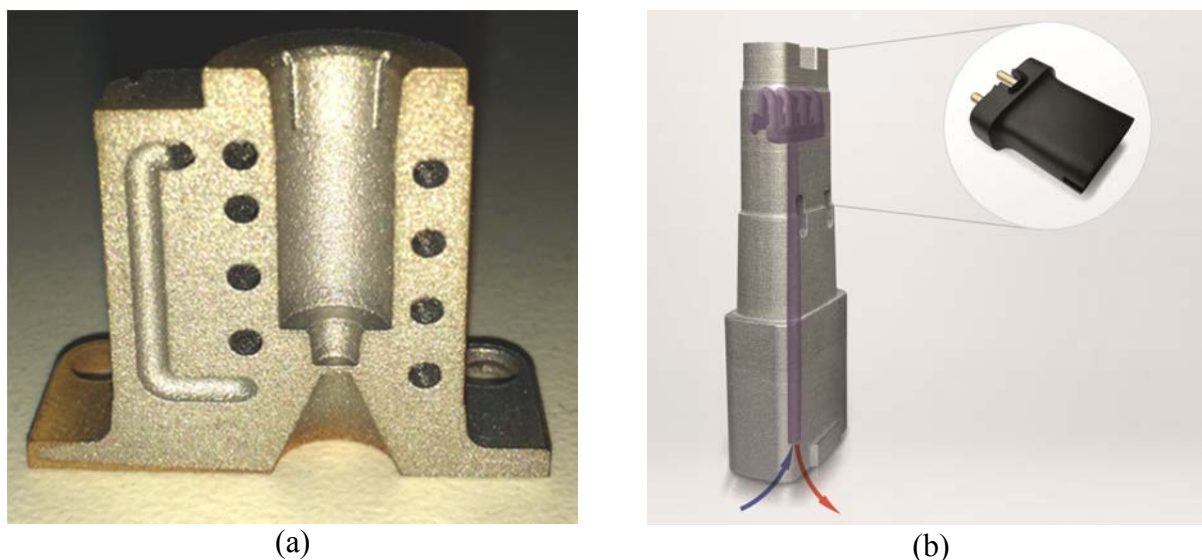
Figure 17.   Injection Molding Tool Examples Representative of Group 3 Complexity
(a) Cross section of L-PBF injection molding tool with internal cooling tubes. *Note this demonstration piece was sectioned in half to demonstrate the production of internal features. L-PBF would be capable of producing both halves as a single component.*
(b) Example of injection molding application which includes internal cooling channels that reduce part cycle time by 43% Image (b) from EOS[41]

4.2.4   Group 4: Design for AM

When a user becomes completely comfortable with AM, they change the way that they look at the design of parts or systems. Design emphasis focuses on optimizing performance without regard to part producibility. These parts can tend to take organic space attributes with very few straight lines or perpendicular corners such as the heat exchanger produced by L-PBF shown in Figure 18.[42]   Such parts are AM Complexity Group 4. Subtractive fabrication is extremely complex as designers begin to eliminate "line of sight" access to features. Subtractive fabrication of Group 4 parts would be prohibitively expensive, requiring multiple intricate machining operations and multiple close tolerance assembly steps followed by additional intricate machine phases. The opportunity for NDE would occur between fabrication process steps.

Figure 18.   Heat Exchanger Produced by L-PBF Representative of Group 4 Complexity[42]

Fabrication of Group 4 parts using traditional subtractive techniques is an order of magnitude more difficult than a Group 3 part. On the surface, there is no obvious fabrication method or clear opportunity for assembly of subcomponents that create features. However, with creative manufacturing and a large budget, it is feasible that a Group 4 component could be manufactured using modern subtractive technology. Because of the high cost of manufacture and very detailed internal and external features, design of Group 4 parts would not occur if fabrication were limited to tradition subtractive methods. Hybrid manufacture, as suggested by Kroll et al. (2013),[39] that combines AM and subtractive manufacture would be the most likely option. These components have greatly reduced inspectability because surface areas have increased and the vast majority of the structure is very detailed and embedded. Currently, established methods of NDE are not capable of inspecting Group 4 components as an assembly. Inspection prior to assembly would be the only acceptable method of NDE.

4.2.5   Group 5: Lattice Structures

A unique aspect of many AM processes is the ability to create very fine features. An example of taking this capability to its limit is the creation of a free-form metallic lattice. Lattice structures are attractive because they can increase the strength-to-weight ratio, offer the ability to tailor stiffness, damage tolerance, and significantly increase the surface area. Figure 19 shows an example of these lattice structures produced by PBF . In addition, they offer the advantage of having the shape of the mesh core optimized for a specific application. Such components have thousands of nodes and can contain many miles of weld in a relatively small area. Parts that have been fabricated using produced metallic lattice structures represent AM Complexity Group 5.

Group 5 parts are produced almost exclusively through AM (techniques to produce metal foams would be one "conventional" example). There is no traditional subtractive technology capable of fabricating a Group 5 component. Internal features, even if separated into assemblies, have no "line of sight" for tooling access. They are complicated and time consuming to manufacture using AM; however, these AM components offer the greatest potential advantage. They also offer the greatest challenge for existing NDE technologies. New or creative application of existing NDE technologies would be required for inspection of Group 5 components. If a method of NDE proves applicable, then usage of a Group 5 part would allow an overall cost reduction at the "system level", meaning that the cost reduction of manufacturing the entire final deliverable offsets the increased cost of fabricating the individual component.
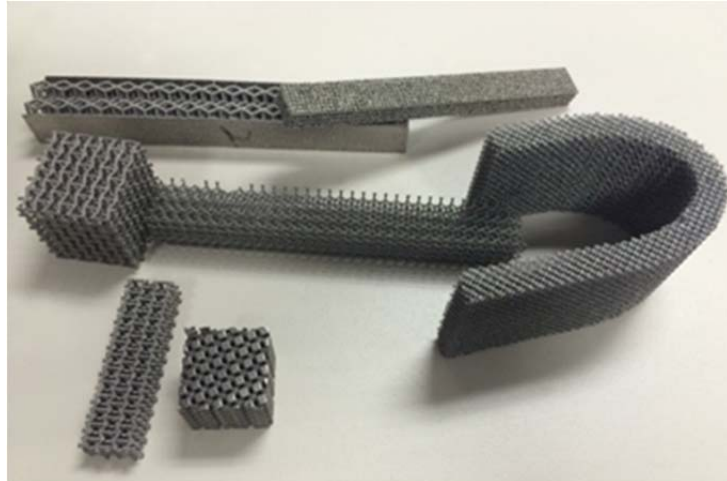
Figure 19.   Metallic Lattice Structures Produced using PBF Techniques, Representative of Group 5

4.3   Nondestructive Inspection Literature Search

Nondestructive inspection methods and techniques for post-production quality assurance or in-service inspection are a necessary component of any manufacturing process. There are multiple methods and techniques available to inspect conventionally produced components in various industrial settings. Several of these methods and techniques have been or may be applicable to components produced by additive manufacturing. Section 4.3.1 is a literature review of industrial techniques that have the highest near- (less than 3 years) and mid-term (3-5 years) potential to inspect titanium and nickel aerospace components produced by PBF techniques. The review also includes nondestructive inspection techniques that have been described in the open literature to inspect metallic components produced by AM. The literature review extends to Section 4.3.2 into the area of medical imaging techniques that could be applicable with further development. These techniques are viewed as having far-term potential, but may provide breakthrough inspection techniques where current industrial techniques fall short.

4.3.1   Industrial Techniques

Table 4 lists industrial nondestructive inspection techniques considered in the assessment and literature review. The ability of each technique to detect different types of flaws such as inclusions, porosity, lack of fusion, and cracks, as well as locate these flaws in the interior or exterior surface of a conventionally manufactured metallic component, is listed. Finally, the techniques are further characterized by the ability to screen or identify and locate a flaw. For additional information, see the references section of this report.

From the list in Table 4, the following techniques were removed for further discussion in the literature section due to their inability to inspect titanium and nickel alloy metallic aerospace components produced by AM:

- Magnetic Testing – Only applicable to magnetic components; the alloys of interest are not magnetic.

- Microwave Nondestructive Testing and Terahertz Imaging – Eliminated on the basis that the materials of interest are electrically conductive.

Table 4. List of NDE Techniques and Characteristics

NDE Technique	Common Acronym	Material and Flaw Types Detected	Surface or Interior	Global Screening or Detect Location
Visual Testing	VT	In any solid material, any condition and/or defect affecting visual light reflection.	Surface	Detects and images location
Leak Testing	LT	Solid material. Discontinuities.	Through thickness	Detects location
Liquid Penetrant Testing	PT	Any solid material. Discontinuities - cracks, pores, nicks, others.	Surface breaking	Detects and images location
Process Compensated Resonance Testing	PCRT	Any solid material. Any defect or condition.	Surface and subsurface	Global screening
Impedance computed tomography or Electrical impedance tomography	ICT or EIT	In electrically conductive material, any condition and/or defect affecting electrical conductivity.	Surface and subsurface	Detects and images location
Alternate Current Potential Drop	ACPD	In electrically conductive material, any condition and/or defect affecting electrical conductivity.	Surface and subsurface	Detects location
Eddy Current Testing	ET	In electrically conductive material any condition and/or defect affecting electrical conductivity, magnetic permeability and/or sensor-part juxtaposition	Surface and slightly subsurface	Detects location
Array Eddy Current Testing	AEC	In electrically conductive material any condition and/or defect affecting electrical conductivity, magnetic permeability and/or sensor-part juxtaposition	Surface and slightly subsurface	Detects and images location
Phase Array Ultrasonic Testing	PAUT	In any solid material, any condition and/or defect affecting sound attenuation, propagation, acoustic velocity and/or sensor-part juxtaposition.	Surface and subsurface	Detects and images location
Ultrasonic Testing	UT	In any solid material, any condition and/or defect affecting sound attenuation, propagation, acoustic velocity and/or sensor-part juxtaposition.	Surface and subsurface	Detects location

NDE Technique	Common Acronym	Material and Flaw Types Detected	Surface or Interior	Global Screening or Detect Location
Radiographic Testing	RT	In any solid material, any condition and/or defect affecting X-ray absorption.	Surface and subsurface	Detects and images location
X-Ray Computed Tomography	X-Ray CT	In any solid material, any condition and/or defect affecting X-ray absorption.	Surface and subsurface	Detects and images location
Microfocus X-Ray Computed Tomography	X-ray MicroFCT	In any solid material, any condition and/or defect affecting X-ray absorption.	Surface and subsurface	Detects and images location
Magnetic Particle Testing	MT	Magnetic material. Discontinuities - cracks, pores, nicks, others.	Surface and slightly subsurface	Detects and images location
Microwave Nondestructive Testing	N/A	In any solid dielectric material, any condition and/or defect affecting dielectric permittivity and sensor-part juxtaposition.	Surface and subsurface	Detects location
Terahertz Imaging	N/A	In any solid dielectric material, any condition and/or defect affecting density and sensor-part juxtaposition.	Surface and subsurface	Detects and images location

4.3.1.1 Visual Testing (VT)

Visual testing (VT) is the most widely used inspection technique.[43] It is usually the first step in any quality assurance NDE process. It involves observing of reflected natural or artificial light of the object surface to detect surface defects or conditions. It can be conducted with a naked eye and simple tools such as a flash light and mirror. Visual inspection can be aided by a wide range of measurement tools and accessories such as measurement and profile gauges. A magnifying glass is recommended where small defects need to be detected. Remote visual inspection with rigid and flexible borescope is routinely conducted on complex structures such as interiors of airframes, aircraft wings and jet engines. Computerized remote visual systems are now commercially available to conduct high resolution visual inspection, data acquisition, digital storage and evaluation. Forsyth et al. discussed the application of several advanced and automated systems for remote visual inspection of aircraft structures.[44]

Enhanced and remote visual systems can be adapted to inspect AM components. Flexible borescope computerized systems can be used for examination of interior of complex geometry AM components where adequate access (e.g., conduit or small opening) is available.

4.3.1.2 Leak Testing (LT)

Leak testing (LT) evaluates the capability of a part or component to prevent the escape or entry of gases or liquids from or into the component. It is required where a gas or liquid leak can lead to contamination, loss of costly material, explosion or other unacceptable failure.[45] The leak

test is conducted to detect a leak and/or measure the leakage rate where some leakage is acceptable. There are multiple techniques to perform the test and a large variety of detectors are used. Some of them involve the use of tracer liquid or gas (e.g., helium).

LT can be used for evaluation of AM components or parts (e.g., heat exchanger valves and fittings) where verification of their gas or liquid tightness is required.

4.3.1.3 Liquid Penetrant Testing (PT)

Liquid penetrant testing (PT) is one of the standard techniques that have been used for testing aerospace components for decades. It is based on the capillary phenomenon where a liquid is drawn into tight discontinuities (cracks, pores) open to the surface via surface tension. Typically, the part is thoroughly cleaned and degreased prior to inspection. For critical aerospace components, the surface may be etched to open fine cracks. A penetrant is applied and removed after a certain (dwell) time. The part is then covered with a developer that acts as a blotter assisting the penetrant seepage out of the discontinuity (if present), and on the surface enhancing the indication and improving detectability. PT is a simple physical process; however, it requires strict adherence to quality procedures and processes to ensure a high detection rate for critical aerospace components and parts. The technique is capable of detecting surface breaking discontinuities. It will image the discontinuity length but will not provide information regarding the discontinuity depth. Experienced personnel and facilities to conduct high quality PT are readily available. Numerous industry studies have been conducted to quantify the PT performance and process robustness. The Center for Aviation Systems Reliability at Iowa State University partnered with the industry in 2001, and conducted one of the largest studies on Engineering Assessment of Fluorescent Penetrant Inspection.[46] Final results were reported at the ATA's 52nd Annual NDT Forum, 2009 in Atlanta, and in other publications during the program implementation. Two of the major factors identified by the study that might affect the performance of PT for AM components were.[47]

- Part Preparation – Cleanliness, metal smear from machining or cleaning, use of etchant, plugging of defects with cleaning media, chemical cleaning process, dryness of part and defects, and previous penetrant inspection.

- Nature of Part and Defect – Surface condition of part, complexity of part, defect type, defect dimensions, and loading condition of part (closure).

All of these and other factors such as surface roughness and removal of the penetrant from AM parts with complex shapes must be addressed when PT is considered for post AM process NDE. The major challenges for applying PT to AM components produced by L-PBF are the as-built surface roughness and line of sight issues. The inherent surface roughness of AM parts due to attached powder creates small crevices where powder attaches to the bulk component (see Figure 13 and Figure 14).[21,25] These crevices allow for capillary action of the penetrant to occur just as a surface breaking discontinuity would, potentially masking actual flaws. While there is not a minimum surface roughness required to apply PT, as with many NDE techniques, the best practice is to determine the effect of a condition (e.g., surface roughness) on NDE response and address this effect through calibration standards mimicking the condition with known defects, procedure controls, and dedicated field trials.

Removal of the penetrant from these rough surfaces after PT is also of concern and is discussed in ASTM Standard E1209-10.[48] Given that as-built surfaces produced by L-PBF may have different roughness based on their orientation, it may be possible that PT could be applied to simple upward facing surfaces. Downward and vertical facing surfaces would not be applicable to PT for most L-PBF techniques. If the parts could be machined components, then it is possible that PT could be applied to L-PBF parts falling into Groups 1-3.

To identify a defect, a line of sight to the possible flaw location is required, thus making PT a poor technique for components having features such as internal cavities, and channels and lattice features characteristic of Group 4 or 5 components.

4.3.1.4 Process Compensated Resonance Testing (PCRT)

The Process Compensated Resonance Testing (PCRT) method for nondestructive evaluation is a standard method used in various industries such as automotive, aerospace, power generation, and others as described in ASTM E2534.[49] To conduct PCRT, a metallic or nonmetallic part is excited at its resonance frequency or several resonance frequencies, and a decision is made whether the part is acceptable or unacceptable based on resonance frequency shift. The resonance frequency depends on the part stiffness and mass. Schwarz, et al. provided examples of PCRT applications where the effects of process variability were compensated (hence, the name) to reduce the false positive calls and improve the technique's reliability.[50] Aerospace components with complex shapes such as engine blades have been successfully tested, as reported by Piotrowski et al.[51] PCRT has been used for in service engine blades, salvaging parts or testing surplus blades. The technique is fast and reliable, if adequately optimized for the application. It is a tool for global testing or screening and cannot reliably discriminate the source of defect indication. Other NDE techniques may be required to conduct more precise defect characterization following PCRT.

4.3.1.5 Contact 4-point Measurements and Electrical Impedance Tomography (EIT)

These contact measurement techniques involve the use of four pins. Two of the pins inject direct (DC) or alternate (AC) current into the part, while the other two pins are used to measure the voltage drop on the part surface. The measured voltage is then divided by the current to determine the electrical impedance that is correlated to the part electrical resistance or conductivity. Electrical resistance can then be correlated to mechanical and other material properties.

For electrically conductive components produced by PBF processes, Boillatt et al.[52] demonstrated a technique for measurement of electrical resistivity to establish correlation with mechanical properties. The electrical resistivity (or conductivity) can be measured with contact (4-terminal Kelvin circuit) or non-contact (eddy current (EC)) techniques used extensively for aerospace applications as discussed later. A DC contact 4-terminal technique was selected. A correlation was established between sintered density and electrical conductivity.

Bogdanov, et al. demonstrated advanced electrical impedance tomography (EIT) for imaging internal and external defects in polycrystalline diamond cutters (PDC).[53,54] The PDC are fabricated by sintering diamond powder onto a tungsten carbide-cobalt substrate. The cobalt acts as a catalyst for bond formation between the diamond crystals. The electrical conductivity (depending on metal content) of the diamond cutter ranges from 100 to 10,000 S/m and it is

strongly correlated with the cutter performance. The PDC are discs with thicknesses up to 4 mm and diameters from 7.6 mm to 25.4 mm. The cutters are positioned in a special holder with multiple pins where two of the pins inject the DC through the PDC thickness and multiple pins are switched to measure the voltage drop. The impedance through the PDC thickness is obtained using an advanced inversion computational technique. The reconstructed impedance images voids, cracks and conditions that might strongly affect cutter performance in service. In the L-PBF of metallic aerospace components, EIT and ICT could be used to detect and image conditions and defects in the volume of small components.

4.3.1.6 Contact Alternating Current Potential Drop (ACPD)

Commercial Alternating Current Potential Drop (ACPD) instrumentation has been developed to measure the electrical resistance and correlate it where relevant to microstructure, residual stresses and others. Madhi and Nagy reported on ACPD resistivity (or conductivity) measurements related to possible microstructural changes due to thermal cycling of Inconel 718 (IN-718) superalloy.[55] A commercial ACPD instrument, LR700, was used where the injection current frequency was set at 16 Hz. Annealed IN-718 specimens were thermally cycled in temperatures from 400º to 800ºC. Along with the well pronounced reversible conductivity versus temperature cycles, irreversible changes of electrical conductivity that could possibly be associated with effects that temperature cycles might have on microstructure were recorded. The irreversible conductivity changes have to be accounted for when ACPD or similar NDE techniques are used for monitoring microstructure of critical aerospace parts in service and during fabrication. It may be possible to correlate conductivity measurements with the quality of heat treatment of AM components.

Madhi, et al. conducted an ACPD study with 16 Hz injection current to investigate the effect of cold working on anomalous decay of electrical conductivity.[56] The unexpected reduction of electrical conductivity was detected when performing eddy current conductivity spectroscopy (ECCS), discussed in Section 4.3.1.7.1 of this report, for residual stress profiling in surface layers of nickel-base superalloys. It was found that the cold work performed on IN-718 caused the thermal relaxation detected with conductivity changes to start earlier than previously thought. The results would be used to enhance the ECCS for residual stress profiling. Mechanical treatment and post processing of AM components during fabrication or in service may induce microstructural changes that could be detected by measuring electrical conductivity with this technique.

The ACPD techniques are directional, and its directionality was used by Prajapati, et al. to investigate creep damage in Cr-Mo-V alloy.[57] The technique is referred to as directional ACPD (DACPD). Isotropic stainless steel 304 and anisotropic Ti-6Al-4V were tested to demonstrate technique performance in detection and resolving small conductivity changes along two orthogonal directions on a plate. The DACPD was able to resolve anisotropy in the range of 4% between the two directions. It is believed that anisotropy down to 1% can reliably be resolved based on experimental results. The approach, however, was difficult to prove for complex geometries like transition from parent metal to welds at the weld toe area where the geometry would have significant effect on the measurements.

4.3.1.7 Eddy Current Testing (ET)

An eddy current (ET) is induced in a conductive material when an alternating magnetic field is brought into close proximity with the material. The alternating magnetic field is usually created by a coil connected to a source of sinusoidal current. The magnetic field of induced eddy currents interacts with the coil magnetic field causing the coil impedance to change. The change of coil impedance is monitored with the EC instrument and depends on material electrical conductivity, magnetic permeability, distance between the coil and material or lift off. Although direct contact between the coil and the material is not required to conduct the test, the EC sensitivity to surface and subsurface discontinuities and conditions is the highest when the distance between the two (lift off) is as small as practically possible.

4.3.1.7.1 Noncontact Conductivity Measurements with ET

Significant research was conducted to validate noncontact ET techniques for evaluation of residual stresses on the surfaces of metallic aerospace components. Residual compressive stresses are introduced into critical aerospace components made from titanium and nickel-base superalloys to improve stress corrosion and fatigue resistance. The process of compressive stress introduction is usually peening, and the electrical resistance or conductivity changes due to the piezoresistivity effect. Sekine and Soyama investigated the use of EC technique for measurement of compressive elastic stresses in austenitic stainless steel 316L.[58] The authors found that the introduction of compressive stresses led to a reduction of electrical resistivity which is measured by EC techniques. This indicated that EC techniques could be used for evaluation of residual stresses in austenitic stainless steels. The approach could be investigated for AM components made of titanium and nickel-based alloys.

Reconstruction of the residual stress profile from EC data was demonstrated by Shen, et al.[59] A model-based approach was used to invert the stress profile introduced by shot peening IN-718 specimens. The surface texture or anisotropy introduced by the shot peening was also accounted for in the reconstruction process. The EC frequencies were swept from 0.4 MHz to 20 MHz to achieve different depth of penetration required for stress characterization through depth. The reconstructed residual stress profile through specimen depth agreed well with the standard stress X-ray diffraction measurements taken after successive removal of top layers.

Hillmann, et al. applied a conductivity measurement technique with EC sensors to build the stress profile after shot peening.[60] A swept frequency range from 100 kHz to 100 MHz was used to implement the ECCS. Two instruments, a precision impedance analyzer and an EC instrument built specifically for the purpose of ECCS, were used in this study to collect data. Residual stress profiles were obtained for IN-718 material, with and without two shot peen, intensities before and after thermal relaxation. The effect of precipitation hardening on residual stress profiles was also investigated. The conductivity correlated with residual stresses was obtained at depths from 50 μm to 500 μm. The advantages of ECCS for fast nondestructive evaluation of residual stresses were demonstrated.

Shot peening conducted on titanium and nickel-base superalloys increases the surface roughness and introduces residual stresses and cold work in the surface layers. To increase accuracy of residual stress profiling with ECCS, Hillmann, et al. investigated various approaches to separate the residual stress from cold work effects on electrical conductivity.[61] Investigation of anisotropy, pulsed EC and specimen heating did not provide desirable results to separate the

stresses from cold working. The use other modalities such as time-of-flight measurements with ultrasonic was suggested to complement the ECCS.

Direct EC sorting and conductivity measurement techniques with conductivity and model-base instruments were investigated by Todorov.[62] Previous experience where electrical conductivity of titanium alloy welds was correlated to variation of hardness due to air contamination was leveraged to investigate the effect of air contamination of reactive alloy welds. Various levels of air contamination in reactive alloys during weld deposition were detected and reliably separated. The degree of contamination was correlated with the electrical conductivity measured with different EC techniques.

4.3.1.7.2   Noncontact Testing for Discontinuities with ET

EC techniques are used extensively for inspection of critical parts and components such as heat exchangers, jet engines, rocket and aircraft structures (e.g., wings, fuselage, engine attachment fittings), automotive axles, valves, chains, bearings and others. Advanced techniques such as imaging, array sensors, computer simulation tools and others have been deployed in the field lately.

Todorov, et al. conducted a study to demonstrate the capabilities of advanced EC techniques for detection and sizing of fatigue cracks in welds.[63] Butt weld specimens were first fabricated and prepared to initiate and grow fatigue cracks at the weld toe. The specimens were raster scanned with a single EC sensor to produce a C-scan (and/or Isometric view) for imaging, detection, and sizing of fatigue cracks. The specimens were fractured after scanning to validate the EC indications. The EC indications (Isometric view) along with fractography sections are shown in Figure 20.
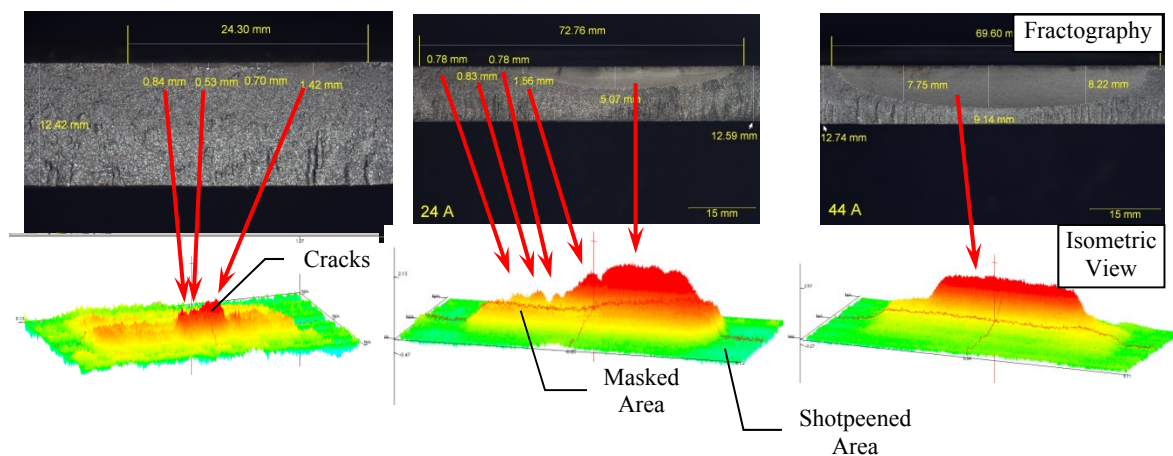
Figure 20.   Fractography (Top) **and EC Indications** (Bottom) **from Three Specimens**

The EC techniques demonstrated very high resolution and sensitivity to small and shallow surface cracks that may occur during AM fabrication. Further, gradual and wide area material changes (shot peened versus not shot peened) were also detected, imaged and separated from the discontinuity indications.

Array EC (AEC) technology was developed and is currently implemented for NDE during fabrication and in-service;[64] and, in some instances may replace PT and magnetic particle testing (MT) NDE. The AEC sensor uses an array of sensors or coils instead of a single coil. It allows fast scanning of a wide area in one, or minimum, passes with minimum interference from mechanical movement. The C-scan (and/or Isometric view) is the standard way of data imaging for AEC, allowing post processing with a wide range of tools (baseline subtraction, filtering, subtraction, addition, scaling or calibration, mixing, rotation, spatial derivative, and others). AEC sensors were developed to inspect parts with complex shapes such as the air foil edge of turbine blades, jet engine disc holes and blade slots and others.

Scanning a long fatigue crack and the surrounding area with AEC is shown in Figure 21.[65] The crack or discontinuity indication is easily detected and separated from the steel property change in front of each crack tip. The EC indications in front of the crack tips are caused by change of magnetic permeability (primarily) and electrical conductivity due to stress, and possibly strain in the ligament areas. An area of 200 × 300 mm as shown on the C-scan in Figure 21 can be scanned and imaged in less than a minute with the AEC sensor.
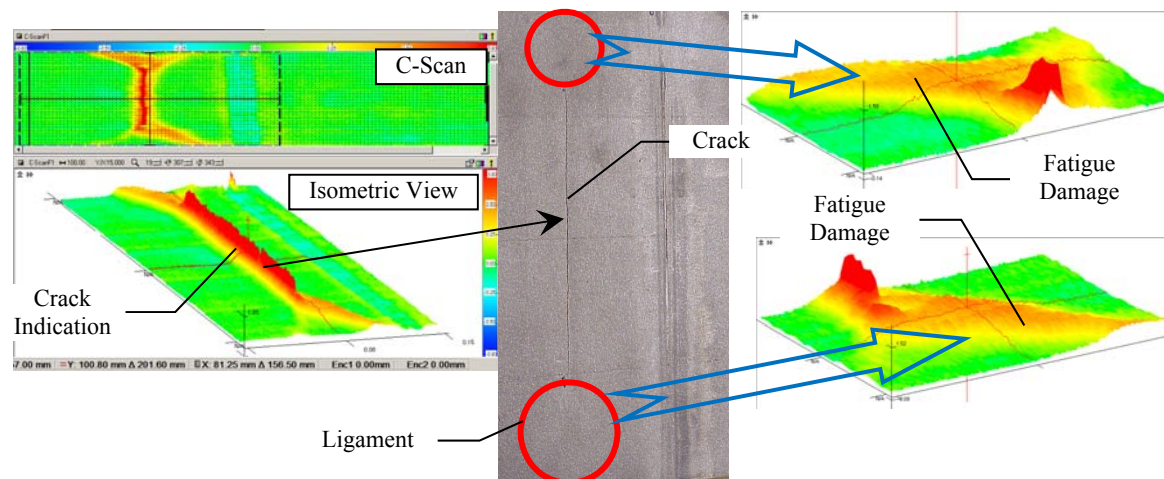
Figure 21. Examination of Fatigue Crack and Surrounding Area with AEC Technique

Further research in EC sensors led to development of flexible AEC[66-68] techniques where the array conforms to the inspected surface, improving the reliability and detection capabilities of the examination. The coils can be printed or etched on a substrate with diameters of approximately 1 mm or smaller. The flexible printed arrays can bend to almost any angle, accommodating complex geometries such as turbine blade attachment slots or "fir trees".

The flexible AEC sensors will possibly provide the best options for examination of AM components with complex geometry. Subsurface defects can also be detected. The detectable size of defects for AM components will certainly depend on access, material, geometry, anisotropy, surface roughness, and other factors.

4.3.1.8 Ultrasonic Techniques for Discontinuity and Microstructure Detection and Imaging
A variety of ultrasonic techniques have been established to examine raw materials and critical components in the oil and gas, energy, heavy and light manufacturing, and aerospace industry

sectors. Ultrasonic technology uses high frequency sound waves, typically in the range of 1 to 15 MHz, to inspect for discontinuities. Detection is primarily accomplished by monitoring sound energy reflected from a discontinuity.

A significant improvement in ultrasonic capabilities and expansion of applications came with the development and deployment of phased array technology.[69] Phased array ultrasonic (PAUT) sensors use multiple elements instead of a single element. The acoustic beam can be formed, steered and focused throughout the component volume and surface electronically for optimized detection and discontinuity imaging. Lately, there is a trend in industry to use advanced ultrasonic PAUT techniques in lieu of radiography especially for detection of planar discontinuities in critical components.

PAUT sensors can be designed and fabricated in many shapes and forms to conform to various geometries and applications as described by Hopkins, et al.[70] Phased array UT (PAUT) and surface-adaptive ultrasound with adaptable or flexible arrays are particularly suitable for complex components.[71-73] A linear (LPA) or matrix phased (MPA) array is made flexible to conform to the contact surface (Figure 22).[73] Multiple combinations of elements can then be grouped in apertures and electronically excited to conduct scanning, and to steer and focus the acoustic beam at areas of interest. The MPA is capable of beam steering in different directions to detect tilted, skewed, and branched defects that are difficult to detect with other techniques. It is also possible to generate multiple presentations of the examined area such as C-, B-, and D-scan in addition to traditional A-scan.
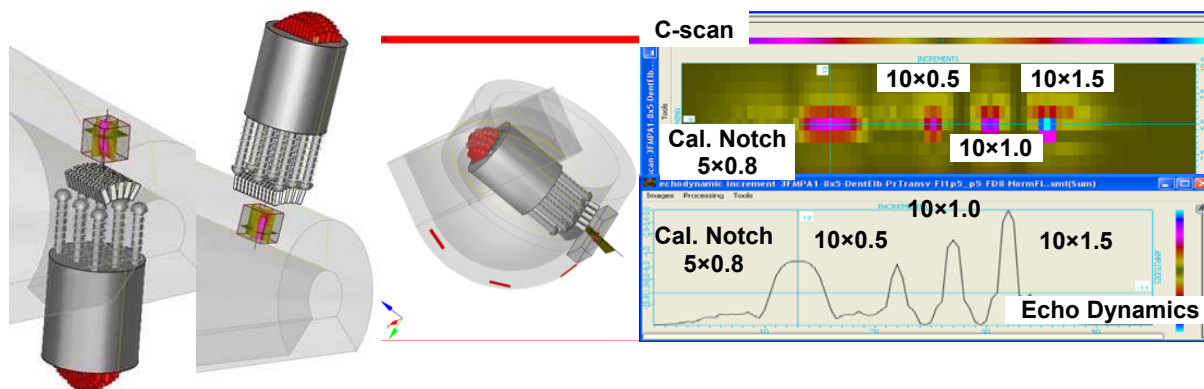
Figure 22.   Example of Flexible Matrix Phased Array Applied on Radiused Features

Recently, Jeong demonstrated the application of advanced time reversal focusing algorithms with flexible array to improve the PAUT capabilities when complex geometries are tested.[74] Jeong also suggested a similar advanced focusing technique for anisotropic and inhomogeneous welds.[75] The approach might be applicable to AM components and parts after adequate research and adaptation.

The formation of a microstructure with high anisotropy may result in the attenuation of the ultrasonic wave and generation of noise during the non-destructive ultrasonic inspection. According to Belway et al.[76] and Nicoletti et al.,[77] there is an inverse relation between attenuation and grain size. Beam attenuation may mask defects, resulting in lower inspection accuracy and reliability. Gorman and Woodfield[78] plotted the influence of anisotropy in the

Distribution Statement A: Approved for public release; distribution unlimited.

microstructure of titanium on the attenuation of an ultrasonic wave (Figure 23a). The effect of grain size of Inconel 718 on the noise generation was studied by Telschow (Figure 23b).[79] The relationship between wave attenuation and grain size can be used as a non-destructive tool to correlate ultrasonic signals to microstructural characteristics of a part. Karthik et al.[80] used ultrasonic longitudinal waves to correlate the wave velocity and attenuation to the density and grain size of 17-4 PH stainless steel produced by L-PBF.

In α+β titanium alloys, α colonies can behave as large grains as well. Therefore, attenuation of ultrasonic wave in titanium alloys is expected. Belway et al.,[76] Gorman and Woodfield,[78] and Paxson and Shamblen[81] developed heat treatment procedures and techniques to generate a microstructure suitable for ultrasonic testing of titanium. Also, it has been reported that twinning in the microstructure of nickel-base alloys with face-centered structure (FCC) could contribute in noise generation and attenuation of ultrasonic waves.
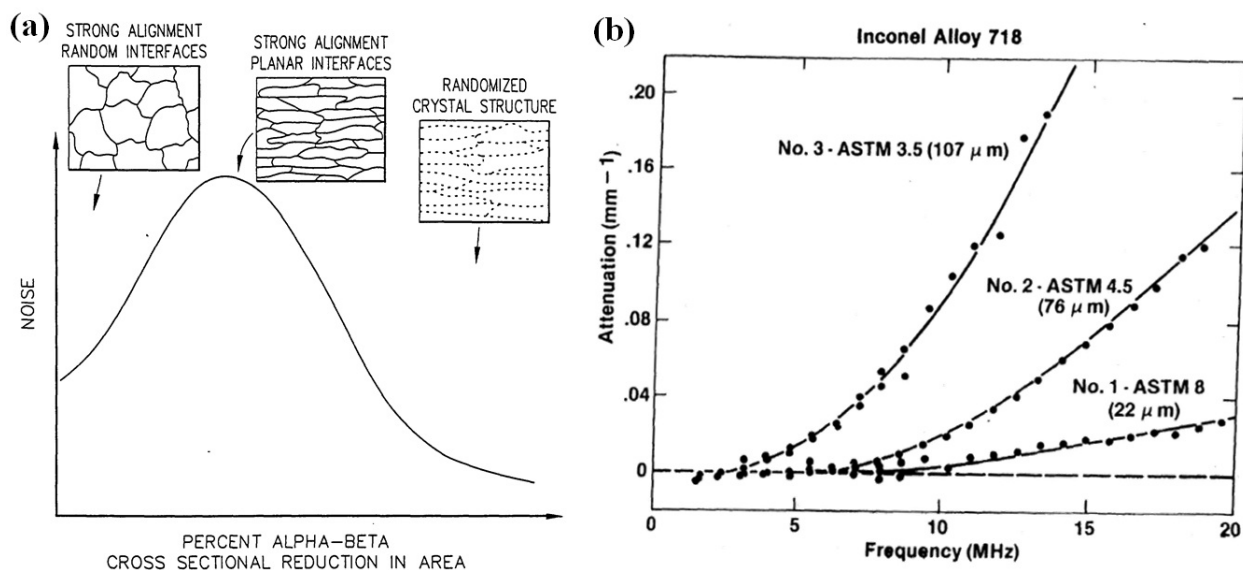
Figure 23. **Schematic of Influence of Microstructure on Attenuation (noise) of Ultrasonic Wave: (a) influence of anisotropy in the microstructure of titanium alloys;[78] (b) influence of grain size of Inconel 718[79]**

As already discussed, AM components will have strong directional anisotropy, and possibly, larger grains, than conventional wrought products. This will cause more attenuation, and possibly, beam skewing which in turn might lead to deterioration of detection and sizing capabilities for small discontinuities.

4.3.1.9 Conventional Radiography Testing (RT)
Conventional Radiography Testing (RT), using either film or digital imaging media, produces two dimensional imaging of components. This could provide useful inspection of Group 1 and Group 2, and limited application for Group 3. As the component cross-section becomes more complex however, abrupt thickness changes will lessen the effectiveness of this method due to difficulty in imaging thick and thin areas simultaneously. Thinner locations will be overexposed when trying to image thicker locations and thick areas will be underexposed when trying to

31

image thin areas. This becomes particularly troublesome when interpreting results at transitions between thick and thin areas. While techniques such as multiple exposures, use of different speed films, and digital enhancement can help, complete useful coverage of complex geometries is not possible with conventional RT.

4.3.1.10 X-Ray Computed Tomography

Industrial computed tomography (CT) scanning technology was introduced in 1972. The objective of CT is to obtain information regarding the nature of a material occupying exact positions inside a body or an object.[82] X-ray CT is the most common form of computed tomography and as such, the acronym " CT" is often used to refer to x-ray CT. The primary components of industrial X-ray CT are a radiation source, a rotational stage, an X-ray detector, and a data processing/image reconstruction center as shown in Figure 24. There are two types of strategies used to produce images in X-ray CT: cone beam and fan/line beam scanning. Fan/line scanners are the first generation of industrial CT scanners and produce X-rays where the beam is collimated to create a line. The X-ray line beam is translated across the part and data is collected by the detector. The data is then reconstructed to create a 3D volume rendering of the part. The cone beam technique uses a cone of radiation as the illumination source and is a collection of Two-dimensional (2D) images acquired as the part rotates in the beam. As the scan progresses, approximately 1300 2D images are collected by the detector. The 2D images are then processed to create a 3D volume rendering of the external and internal geometries of the part.[83]
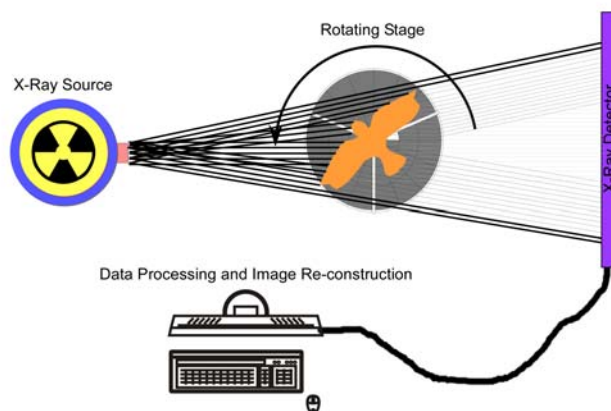
Figure 24. Schematic of X-ray Computed Tomography

4.3.1.10.1 Radiation Source

The x-ray source for CT has several attributes that determine the effectiveness of the technique. These attributes include, but are not limited to, radiation power, emitter spot size, wavelength, and beam type (fan or cone). The thickness of an object that can be effectively imaged while performing a radiograph is related to the density of the material, amount of material present, and the energy level of the radiation being produced. Commercially available CT scanners fall within the range of 100 kv to 450 kV. General Electric rates the power of their CT scanners in watts, with the maximum power ranging from 15 Watts for the Nanatom™ to 1500 Watts produced from the v|tome|x™ L 450.[84] The two orders of magnitude differences in power indicate the type of reconstructions to be obtained from the scan. X-ray CT units capable of

higher power are generally used to scan thicker more dense parts, while units operating at lower power can be used to scan less dense materials and will often use a radiation source with a small emitter size to obtain resolutions down to the sub-micron scale. These small spot size sources are often referred to as Fine Focus™ or Micro Focus™ tubes. There are others, but the principles of small spot size X-ray sources are the same. Microfocus tubes use a regenerated jet of liquid metal as anode which relaxes the limitation at high e-beam power density. These tubes generate X-ray radiation using liquid metallic targets instead of solid tungsten as shown in Figure 25.
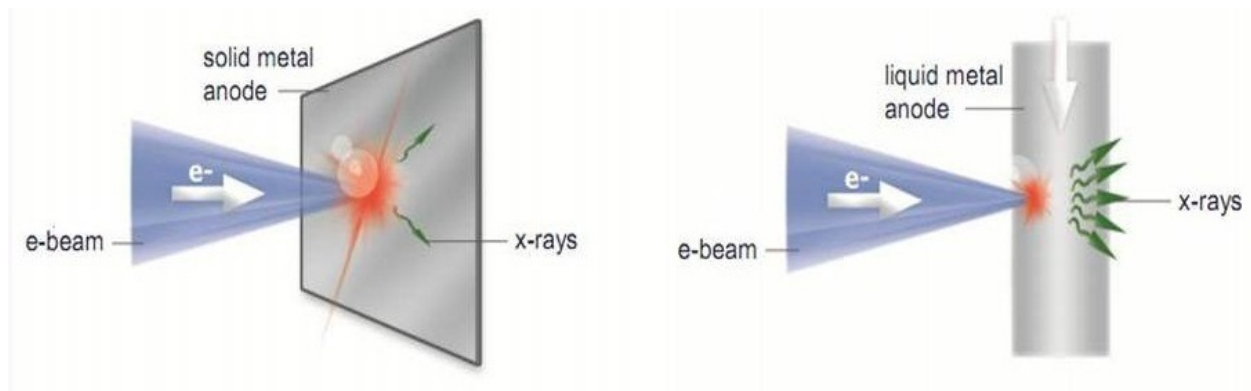
Figure 25. Diagram of Solid Metal Anode and Liquid Metal Anode

These sources are currently being operated at an e-beam power density of 600-1300 kW/mm2 (7-20 μm spot size),[85] and there is potential for significant increase. For PBF fabricated components, a small spot size radiation source is desirable due to the small features and defects expected to be found in the build.

The effect that the emitter spot size has on the quality of the CT image is significant, primarily due to the phenomena known as geometric unsharpness or penumbra. Geometric unsharpness refers to the loss of definition that is the result of geometric factors of the X-ray CT equipment and setup. It occurs because the radiation does not originate from a single point but rather over an area as illustrated in Figure 26. These, along with source-to-object distance and source-to-object detector distance, are the three factors that control the sharpness of a CT scan.[86]

Distribution Statement A: Approved for public release; distribution unlimited.

Geometric Unsharpness - Ug
(Penumbra)

Larger Finite Source

Point Source

Ug = f * b/a
f = Source focal spot size
a = Source to object distance
b = Thickness of object

a

a

Object

b

b

Ug

Ug

Penumbra (Ug)
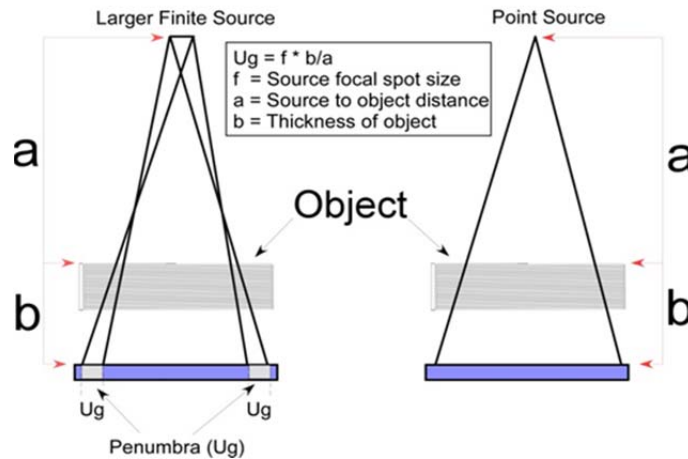
Figure 26. Illustration of Geometric Unsharpness

This effect is an important consideration when performing X-ray CT because object placement relative to the radiation source and image collection device can have the effect of magnification of the object being scanned (Figure 27 and Figure 28).[86] The magnification due to the geometry of the radiographic set-up is expressed by:

$$M = \frac{O_1}{O_2} = \frac{(D_1 + D_2)}{D_1};$$

M = Geometric Projection Magnification
$O_1 = Width\ of\ object$
$O_2 = Width\ of\ Projection$
$D_1 = Source\ to\ Object\ Distance$
$D_2 = Object\ to\ Image\ Plane\ Distance$

Source

$$Magnification = M = \frac{O_1}{O_2} = \frac{(D_1 + D_2)}{D_1}$$

D_1

O_1

Object Plane

Object

D_2

O_2

Image Plane

Enlarged Image
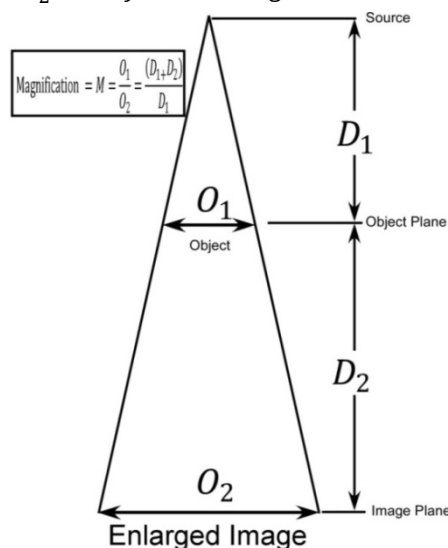
Figure 27. Magnification

34
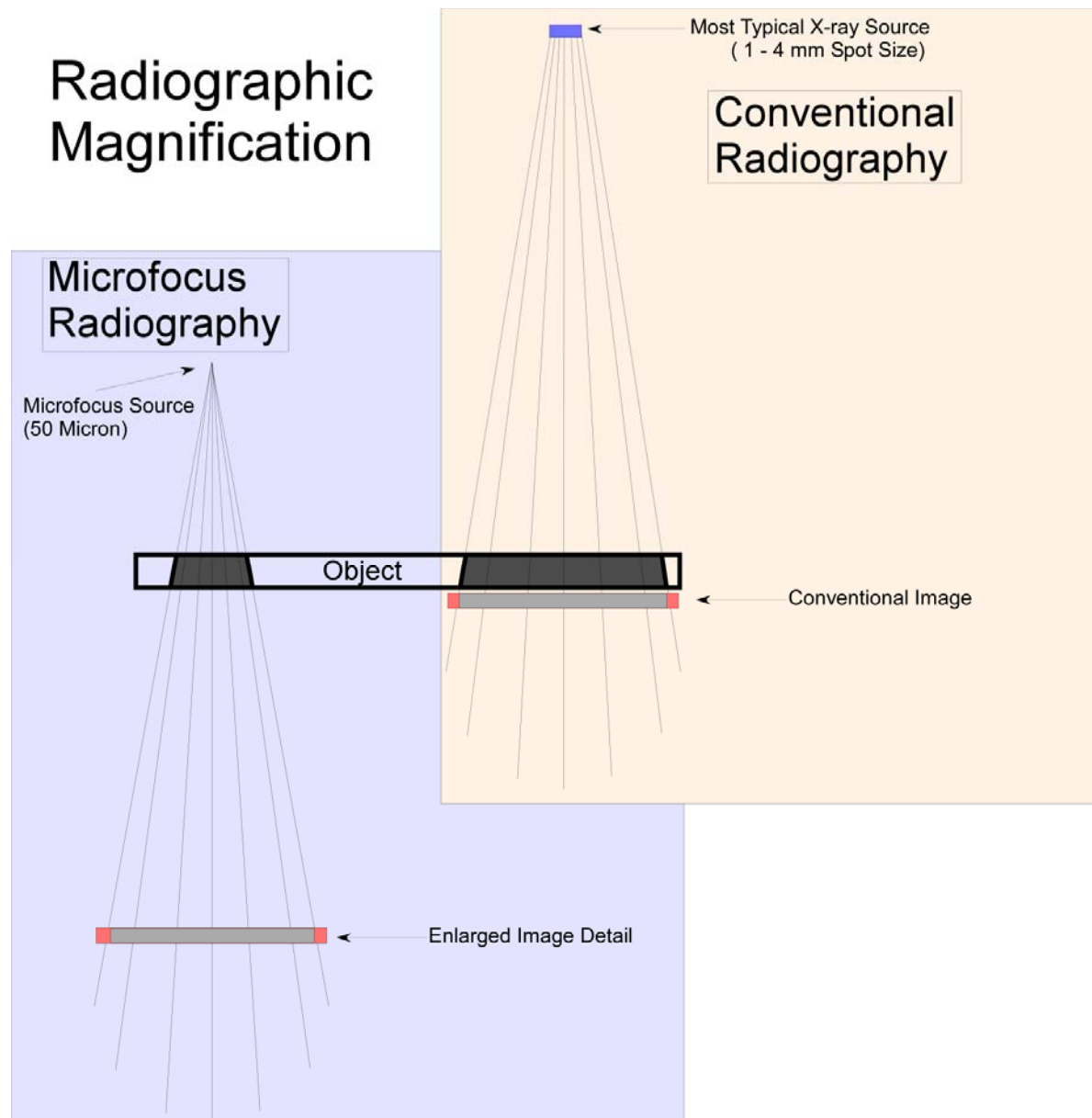
Figure 28. Comparison between Conventional Radiography and Microfocus Projection Radiography

This can be advantageous when scanning PBF parts with layer thicknesses at the 20 to 40 μm level. Some of the smaller spot size CT units have resolutions as small as 500 nm.[87] The size of the device producing the ionizing radiation is proportional to the amount of energy that can be used to collect data. For thicker, denser, complex PBF-based structures, it becomes more difficult to use a micron sized emitter to produce the CT image. Interestingly, Nikon manufactures a microfocus X-ray source that has an operating voltage of 750 kV, a continuous power rating of 750W, and a voxel size of down to 30 μm. The material penetration is approximated at 160 mm for aluminum and 60 mm in steel, giving significant capability for thicker, more dense builds. Some of the more recent CT machines use dual spot size sources to

Distribution Statement A: Approved for public release; distribution unlimited.

accommodate the requirement of different thicknesses and densities. These units have a large spot size radiation source for higher power application and a microfocus source for thinner, less dense parts. If the spot size for these types sources continue to reduce, the limitations of CT as it applies to PBF components will not be tied to resolution or thickness of the fabricated component.[88]

4.3.1.10.2 Resolution

The data produced in any type of X-ray CT eventually gets processed to produce a 3D attenuation or density map. This map consists of individual volume elements called voxels that are analogous to a pixel in 2D X-ray (as shown in Figure 29). Each voxel is composed of x, y, and z coordinates along with the X-ray attenuation data. The resolution capabilities of industrial CT system are described by the size of the voxel the system can resolve. For instance the GE v|tome|x s has both macrofocus and microfocus sources installed as a unit. The maximum voxel resolution of the unit is published as less than $2 \times 2 \times 2$ µm for the macrofocus tube, and less than 1x1x1µm using the microfocus capabilities.[87] Nikon's XT H series of industrial microfocus CT units have a voxel resolution of $3 \times 3 \times 3$ µm for the XT H 160kV/60W system to 80 µm resolution for the 450kV/450W product. The XT H 450 has the option of using a "High-Brilliance" X-ray source. "High Brilliance" is a marketing term used to describe X-ray sources that use liquid metal targets.[89] For the inspection of PBF-produced components with 40 µm layer thicknesses, it is important to have an inspection system that has the capability to resolve details of at least half that dimension, or 20 µm.
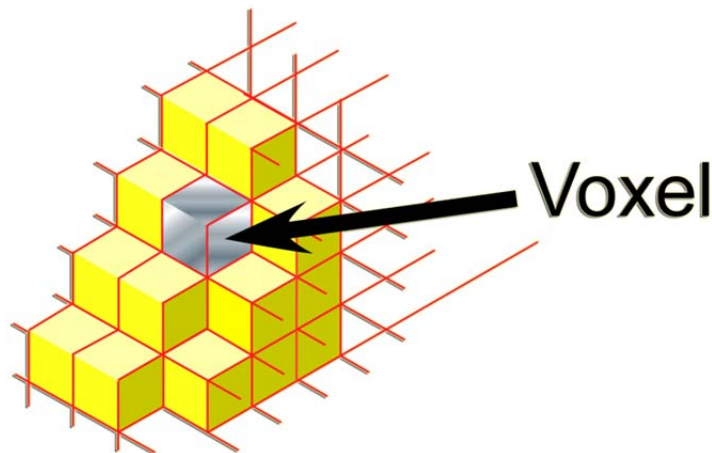
Figure 29. Schematic of Volume Element or Voxel

4.3.1.10.3 X-Ray Detection

X-ray CT is a summation of tens to thousands of individual 2D density maps reconstructed to form a 3D image. A primary technological advancement that has enabled the progression of this technology is the ability to directly digitize the attenuated X-ray beam using solid-state panels similar to the device used to produce images in a digital camera. The size of each pixel, element sensitivity and the physical size of the panel are the primary factors that dictate the maximum size of an object to be tested. The two most important types of detectors currently on the market are devices that convert photons to electrical signals using amorphous silicon (a-Si TFT) which is considered a charged couple device (CCD) and detectors based on complementary

36

metal-oxide-semiconductor (CMOS) technology. Both types of imagers convert light into electric charge and process it into electronic signals. In a CCD sensor, every pixel's charge is transferred through a limited number of output nodes to be converted to voltage, buffered, and sent off-chip as an analog signal. All of the pixel can be devoted to light capture, and the output's uniformity (a key factor in image quality) is high. In a CMOS sensor, each pixel has its own charge-to-voltage conversion, and the sensor often includes amplifiers, noise-correction, and digitization circuits, so that the chip outputs digital bits. These other functions increase the design complexity and reduce the area available for light capture. With each pixel doing its own conversion, uniformity is lower, but it is also parallel, allowing high total bandwidth for high speed.[88] The TFT (CCD) technology is considered far inferior to crystalline silicon CMOS technology in terms of the speed, stability, noise susceptibility, and feature size.[90] While a-Si TFT CCD technology is versatile and manufacturable in large areas, it suffers from high read noise from combined pixel and line noise sources, pixel-pitch limitations, and resistance to lowering manufacturing costs.[88] Perkin Elmer produces a line of flat panel X-rays suitable for X-ray CT that have a pixel resolution of up to 3888×3072, and the ability to generate images at a rate of up to 191 frames per second.[82]

4.3.1.10.4 Data Processing and Image Reconstruction
The feature that makes X-ray CT a powerful and effective tool for nondestructive testing of Group 3 and Group 4 components is the utilization of a significant amount of X-ray 2D image data to reconstruct a precise 3D volume rendering.[91] These renderings can be so precise that they have found uses in metrology for verification of internal feature dimensional tolerance verification. For high resolution images constructed using millions or billions of voxels the limiting factor is scanning speed, and the ultimate large-scale usefulness of the technique is data processing or the ability to turn the data into an image reconstruction.

The mathematical basis for tomographic imaging was discovered and proven by Johann Radon in 1917 and is known as the Radon Transform. This formula forms the basis of tomography and the creation of an image from the projection data associated with cross-sectional scans of an object. If a function f represents an unknown density, then the Radon Transform represents the projection data obtained as the output of a tomographic scan. Hence, the inverse of the Radon Transform can be used to reconstruct the original density from the projection data, and thereby, it forms the mathematical underpinning for tomographic reconstruction, also known as image reconstruction.[91]

The assumptions made for constructing the theory reconstruction based on fan beam or slice data are: 1) the slices are infinitely thin; and, 2) all X-ray photons travel in a straight line, which lie in the infinitely thin slice. Since the slice is infinitely thin, it can be thought of as a picture whose grayness at any point (x, y) is proportional to the relative linear attenuation $\mu_{e(x,y)}$ at that point.[91] The implication is that the distribution of the relative linear attenuations in an infinitely thin slice is uniquely determined by the set of all of its line integrals. This is an idealized mathematical form that poses the following problems when applied to real-world image reconstruction of X-ray CT data.

- Radon's formula determines an image from an infinite set of line integrals. In X-ray CT, only a finite set of measurements are available.

- The measurements in CT can only be used to estimate the line integrals. Inaccuracies in line integral estimates are caused by the width of the X-ray beam, scatter, hardening of the beam, photon statistics, and detector inaccuracies.

- The formula is not a fully vetted and efficient algorithm that produces volumetric images from X-ray CT data. There has been a great deal of effort to find algorithms that are fast, efficient and still produce acceptable reconstructions despite the finite data set and the inherent inaccuracies associated with the data collection process.

The Radon Transform is the basic and founding mathematical principle of image reconstruction. The actual execution of these principles is computationally challenging. This coupled with the amount of data that is produced when scanning at the resolutions required to properly interrogate parts, that have 40 μm build heights and produce gigabytes of data per scan, resulting in long cycle times. To minimize the time it takes to scan and evaluate a Group 3 or Group 4 components, advances in computational power have been applied to X-ray computed tomography.

There are several algorithmic applications of the mathematics that are currently used for image construction. These include but are not limited to:

- Feldkamp algorithm[92, 93]
- Algebraic Reconstruction Technique[92, 94]
- Simultaneous Iterative Reconstruction Technique (SIRT)[92]
- Maximum Likelihood-Expectation Maximization (ML-EM)[92]
- Ordered Subsets Convex Algorithm (OSC)[92]

Research into image reconstruction algorithms is ongoing, and each manufacturer of industrial CT units has their own approaches and optimizations they incorporate into their product line. These optimizations are the requirements of the hardware they will produce, and the perceived application of the unit.

The amount of computational power required to produce volumetric reconstructions in a timeframe that is useful in a production environment is significant. The development of multi-core processors and high performance graphics processors optimized to perform volumetric reconstructions has led to relatively inexpensive but powerful computing clusters. These clusters are composed of nodes. An example of a node composition that was recently used to perform volumetric reconstruction using advanced algorithms is:

- Two 6-core CPUs (Intel Xeon X5650, 2.67 GHz)
- 72 GB RAM
- Two 448-core GPUs (NVIDIA Tesla M2070, 6 GB RAM)
- 2 Terabytes of local storage

This particular cluster system was comprised of 60 compute nodes and had 192 terabytes of system storage. This was able to process reconstructions with up to two billion data events in under 10 minutes.[95] For Group 3 and Group 4 PBF components, miles of weld can be used to produce a single component. Scanning these parts at the resolutions required to detect the small

discontinuities generates many megabytes of data to be processed. For example, to test a cross section of a typical aerospace airfoil with CT might require an image slice of 1024×768 pixels. To test the entire airfoil would require 1024 of these slices to create a $1024 \times 768 \times 1024$ (768 Mb) voxel data set.[96]

4.3.1.10.5 Artifacts in X-Ray CT

Beam Hardening and Scatter

The most commonly encountered artifact in X-ray CT scanning is beam hardening, which causes the edges of an object to appear brighter than the center, even if the material is the same throughout. The artifact derives its name from its underlying cause: the increase in mean X-ray energy or "hardening" of the X-ray beam as it passes through the scanned object. Because lower-energy X-rays are attenuated more readily than higher-energy X-rays, a polychromatic beam passing through an object preferentially loses the lower-energy parts of its spectrum. This results in a beam that, though diminished in overall intensity, has a higher average energy than the incident. In X-ray CT images of sufficiently attenuating material, this process generally manifests itself as an artificial darkening at the center of long ray paths, and a corresponding brightening near the edges. In objects with roughly circular cross sections, this process can cause the edge to appear brighter than the interior, but in irregular objects it is commonly difficult to differentiate between beam hardening artifacts and actual material variations.[84] Manufacturers of CT units employ staggers to account for this phenomenon.

Ring Artifacts

An uncalibrated or defective detector element creates a bright or dark ring centered on the center of rotation. Usually, recalibrating the detector is sufficient to fix this artifact, although occasionally the detector itself needs to be replaced.[84]

Partial Volume Effects

Because each voxel in a CT image represents the attenuation properties of a specific material volume, if that volume is comprised of a number of different substances then the resulting CT value represents some average of their properties. This is termed the partial-volume effect. Furthermore, because of the inherent resolution limitations of X-ray CT, all material boundaries are blurred to some extent, and thus the material in any one voxel can affect CT values of surrounding voxels. Although these factors can make CT data more problematic to interpret quantitatively, they also represent an opportunity to extract unexpectedly fine-scale data from CT images.[84] This artifact would be significant as the ratio of surface area to bounding box area increases, such as in Group 4 and 5 components.

Noise

Poisson noise is due to the statistical error of low photon counts, and results in random thin bright and dark streaks that appear preferentially along the direction of greatest attenuation. This can be reduced using iterative reconstruction, or by combining data from multiple scans. Noise reduction techniques enable inspection scans at a much lower radiation dose. With iterative reconstruction, low dose results in decreased resolution, with only a slight increase in noise.

Metal Artifact

Metal streak artifacts are caused by multiple mechanisms, including beam hardening, scatter, Poisson noise, motion, and edge effects. The Metal Deletion Technique (MDT) is an iterative technique that reduces artifacts due to all of these mechanisms.[84]

Examples of X-Ray CT in Industry

Among all of the available non-destructive techniques, X-ray CT is being widely used for complex manufactured components, including metal castings and additive manufactured components. De Chiffre, et al. recently reviewed a list of industrial applications of computed tomography.[97] Kruth, et al. reviewed the use of CT to verify dimensional accuracy of components.[98] In the early 1990s, the Air Force sponsored the Advanced Development of X-Ray Computed Tomography Applications program, which applied the technique to a variety of applications including ceramics, honeycomb structures, and metal castings.[99-102] Georgeson, et al. previously evaluated X-Ray CT for titanium castings and found that the technique.[101]

- Allows a quantitative engineering evaluation of castings for internal defects, porosity content, 3D location of features, and internal and external dimensions.

- Was found to be more reliable than conventional RT for inspection of critical regions of complex castings. In thick sections (> 0.12 mm) CT imaging may be more sensitive to volumetric defects than radiographic inspection, with respect to MIL-STD-453 requirements.

- Allowed nondestructive internal and external dimensional measurements to an accuracy better than 0.05 mm (0.002 in.).

- Provides valuable data for engineering assessment such as finite element analysis and casting model verification.

- Was found to be cost effective for foundries.

The inspection of complex castings serves as a conventional example to apply CT to PBF components. There are limited examples of application of X-Ray CT to detect internal metallurgical defects such as porosity and lack of fusion in additive manufactured components. For example, Neira Arce[103] used the micro-computed tomography technique for the non-destructive inspection of porosity in Ti-6Al-4V cubes fabricated by EB-PBF (Figure 30a,b). Similarly, Leuders et al.[104] used this technique for the detection of defects in a bar produced by selective laser melting (Figure 30c). Attar,[25] used the computed tomography technique to reconstruct a Ti-6Al-4V thin wall (Figure 30d). Radovan, et al. applied X-Ray CT to scan a patients cranium in order to produce a Ti-6Al-4V implant.[105] Once produced using L-PBF, the implant was scanned using CT for geometric accuracy and defect content. Porosity as small as ~200 μm diameter were not detected in the material.
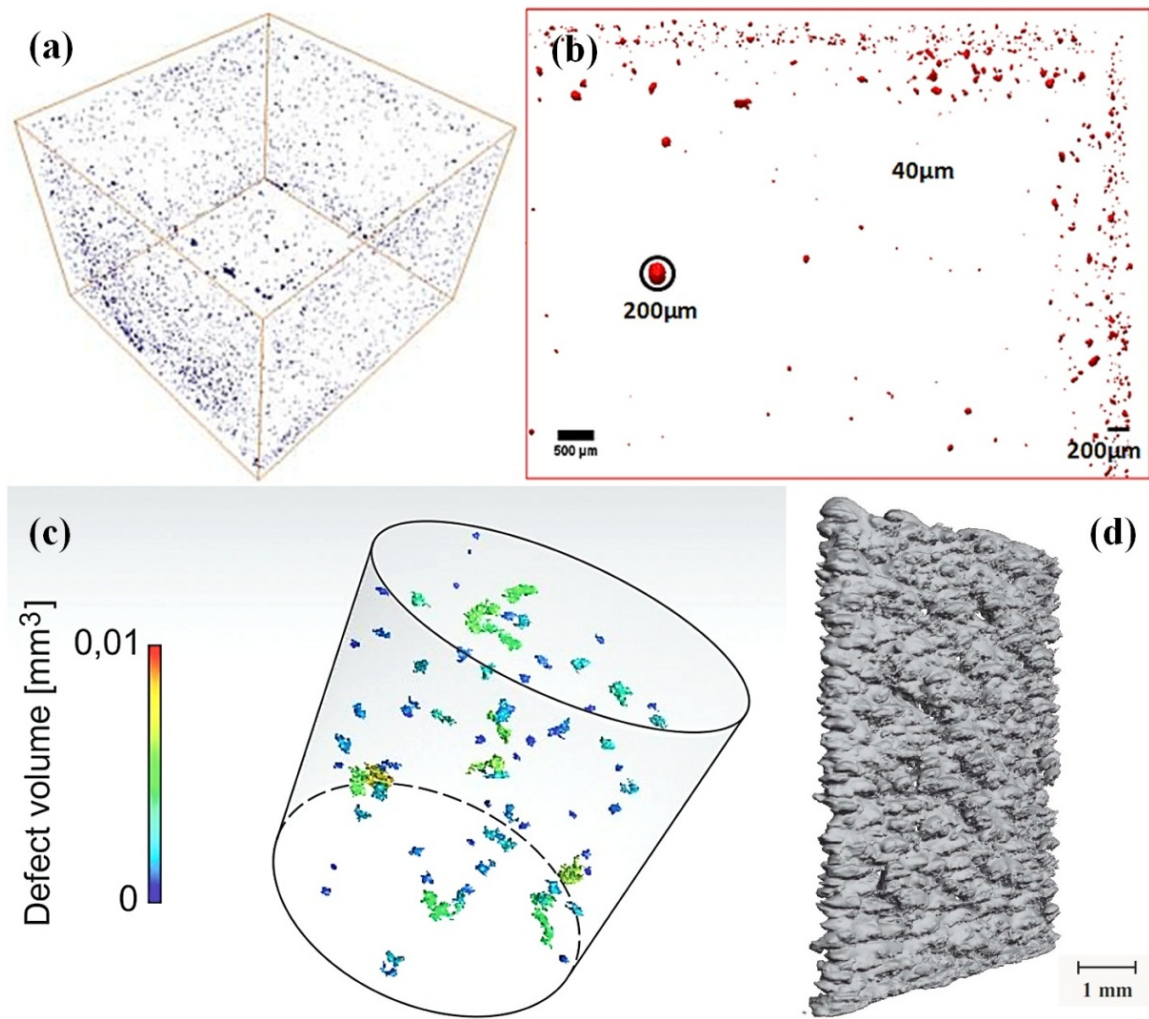
Figure 30. Application of X-ray Computed Tomography (CT) as Nondestructive Technique: (a) 3D view of porosity distribution in Ti-6Al-4V cube fabricated by electron beam melting; (b) Zoomed image of (a) at a 2D view; (c) defect detection in a bar produced by selective laser melting; and, (d) 3D digital reconstruction of thin wall fabricated by electron beam melting

X-Ray CT is accepted as the leading post-processing inspection method for Group 3 and Group 4 components. Given the right combination of equipment and materials, detection capability has been reported that is similar to the powder particle size.[106] This technology is mature and readily available, and has the capability to inspect at the detail needed to validate complex metallic structures. What is not as clear is how well these systems can detect discontinuities in these structures. The question of what the probability of detection is for these systems remains largely unknown.

4.3.2 Medical Techniques

The focus of this task was on finding interesting techniques from the medical imaging field that might be applicable to AM, albeit in the far term. The medical field has helped develop technologies such as phased array ultrasonics and X-ray CT into tools that are useful for industrial NDE applications. It is logical to look at current medical technology for techniques that may have future potential for AM. To limit the scope of the research, it was assumed that the primary interest was on Group 4 components. Because these structures are complex with so many structures and features embedded, most contact methods would provide very little information concerning these internal features. The only practical approach is a through-transmission or internal emission of energy, and a reconstruction of the part based on the transmission/emission paths and energy absorbed, or transmitted by the part. These requirements dictate that a tomographic approach is the one most likely to provide the information needed for part validation. Interestingly, because the human body is complex, significant research has been accomplished in this area.

From the medical perspective, tomography is defined as any method that produces images of single tissue planes. In conventional radiology, tomographic images (body-section radiographs) are produced by motion of the X-ray tube and film, or by motion of the patient that blurs the image except in a single plane. In reconstruction tomography [computerized tomography (CT) and position emission tomography (PET)], the image is produced by a computer program.

In the medical field, there are three different types of tomography:

- Through Transmission
- Pulse-echo
- Emission

4.3.2.1 Through-Transmission Techniques

Through transmission includes techniques such as X-ray CT, Compton Camera Base Tomography, and Fine Focus Tomography (Figure 31). These techniques all use ionizing radiation and are based on the physics of transmittance. Factors such as the size of the transmitting spot size, the energy level of the ionizing radiation, size and sensitivity of the detectors, quantity of data produced, size and relative density of the part being inspected all dictate the effectiveness of the techniques.[91] The limitations of these techniques are in sensitivity to density changes and processing speed. To address these issues, a system with the capability to use different ionizing energy levels and fuse these data to create one coherent scan could be developed. Better sensors and faster data processing will all contribute to continuing improvement of the technology.
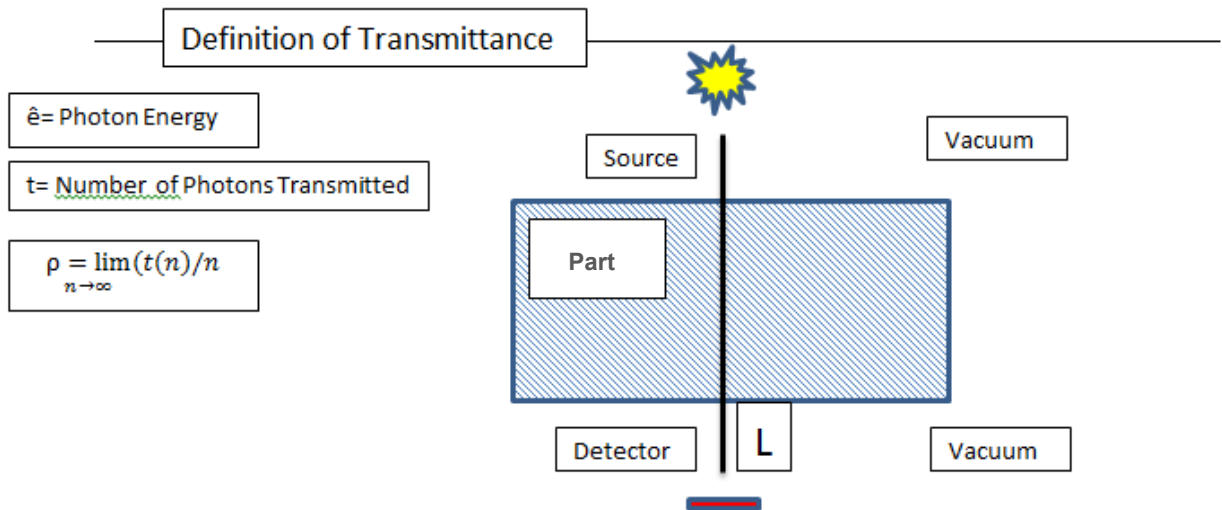
Figure 31. Schematic of Through-Transmission Techniques

4.3.2.2 Pulse-Echo Tomography

Pulse-echo tomography relies on the fact that a given pulse of energy can be reflected and refracted in a material (Figure 32). These data can be used to reconstruct an image of the interior of a part or component and associated defects. One of the more interesting and relevant techniques that use this methodology is ultrasound transmission tomography (UTT). UTT is a technique used to image breast tumors and uses three different properties of sound: velocity changes, reflection, and attenuation. These measurements are taken independently of each other, then the data is fused to develop the final 3D image.[91] It is possible that an AM complexity Group 4 part or component could be immersed in a device similar to Figure 33 and scanned in three dimensions. Pulse-echo techniques applicability is limited in effectiveness to high group number application due the different layering and geometry effect. The actual application of UTT would require significant development and feasibility testing. There are at least two possibilities of advancing the sensitivity of UTT, making it more appropriate for complex metallic structures. The first is changing the coupling medium for the ultrasonic immersion chamber to something that is a closer acoustic impedance match to the material being inspected. What this might allow is better sound attenuation between multiple layers of the AM Group 4 enabling possible interrogation of the layering. The other technique would use MPA to dynamically focus a beam through the part or component.
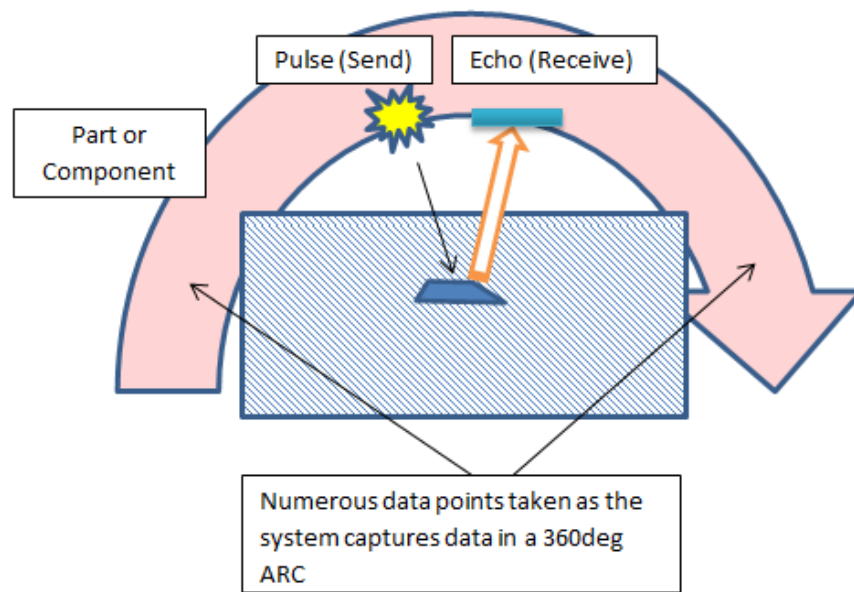
Figure 32.   Pulse Echo Technique

Figure 33.   Ultrasonic Transmission Tomography Medical Device

4.3.2.3 Emission Tomography

When specific location information is required in the human body to get high-resolution images of features, radioactive compounds can be ingested that emit ionizing radiation at a certain energy level. This radiation can be detected using a system of specialized sensors; an image can be constructed from this information. Techniques that use this type of imaging are positron emission tomography (PET) and single-photon emission computed tomography (SPECT). A PET scan uses a small amount of radioactive material (tracer). The tracer is administered to the patient intravenously and travels through the blood and collects in organs and tissues.[107] This helps the radiologist see certain areas of concern more clearly.[108] Like PET, a SPECT scan is a type of nuclear imaging test, which means it uses a radioactive substance and a special camera to create 3D images. Commonly used radioisotopes in SPECT are technetium-99m and iodine-123,

which emit gamma-rays of energies 141keV and 159keV, respectively.[109] These gamma-rays are emitted from the organ of interest and are detected outside the body by detectors, providing an image of the distributed radiation.[110] The fundamental difference between the two techniques is that the PET scan relies on radiopharmaceuticals that emit positrons which convert to gamma radiation that is then detected.

The reason that these two techniques are mentioned in this report is because there are no known emissive tomography techniques for metallic structures. In traditional NDE, the process of fluorescent penetrant testing could be considered an emissive technique where the penetrant collects in areas (cracks) where the capillary action is greater than the surface tension of a defect. It may be possible to have an emissive technique for AM Complexity Group 4 components similar to PT, but using special radioactive liquids with the appropriate half-life and ionizing radiation energy levels. Considering that standard X-ray inspections are performed on typical industrial components at energy levels from 100 to 150 kV, it seems feasible that an energy level of 141keV of technetium-99m should provide suitable penetrating power for many components. What is yet to be determined is the exposure time to generate an image based on energy levels of the medical grade radioactive liquids. If a suitable liquid could be identified, then it might be possible to use techniques like PET of SPECT in conjunction with X-Ray CT to increase the information from the inspection.[111]

It is apparent that emission techniques would only be for possible future consideration since there are currently many unknowns that would need to be considered. Some major unknowns include: how to put liquids or other emissive materials in AM parts during the build process without adversely affecting the component properties; and, how to protect emissive materials from degradation during the build and subsequent operations prior to inspection. One possible alternative is to submerge the completed component in a bath of emissive material–but, this approach introduces a number of other questions which are equally as challenging, such as will the material be able to flow inside the component to highlight internal defects.

5.0 RESULTS AND DISCUSSION

The objective of the study conducted was to define NDE techniques capable of detecting defects in complex geometries and aerospace-relevant materials produced using L-PBF processes. The study has identified several constraints placed on the selection of capable nondestructive inspection techniques, which include the L-PBF process, the component, and the limitations of the NDE techniques themselves. Each of these constraints will be discussed in the following sections, followed by a down-selection of likely techniques that could be used to inspect Group 4 and Group 5 titanium or nickel components produced by L-PBF. Next the current technical gaps are listed and finally, a recommended methodology to address these technical gaps is presented.

5.1 Constraints from L-PBF Process

The two principle characteristics of the L-PBF process that constrain the inspection technique are the diameter of the energy source and the particle size distribution of the metal powder. As shown in Table 3 for commercially available L-PBF systems, the laser beam diameter at focus is on the order of 100 μm while the powder size typically ranges between 20 and 50 μm. Defects present in L-PBF processes can include planar and volumetric defects. Planar defects can include cracking and also lack of fusion (high aspect ratio). Volumetric defects can include porosity and lack of fusion. It is evident from Figure 9 that the size of porosity and lack of fusion defects is on the scale of the beam diameter and powder diameter (Table 3) or less. The defects present are then on the order of 100 μm or less.

The size of the powder used in the process is also primary factor in determining the surface roughness which can affect NDE techniques that interrogate the surface such as PT, VT, ET, AEC, UT, PAUT and others. A final constraint is the effect of the process on microstructure formation. Microstructures in L-PBF of Ti-6Al-4V and nickel alloy 718 tend to exhibit long columnar grains that form during solidification. This can produce anisotropy in the microstructure, resulting in varying levels of attenuation in transmission techniques such as ultrasonic testing.

5.2 Constraints from Components

The components produced by L-PBF constrain the available nondestructive inspection techniques for two reasons. Group 4 and 5 geometric complexity which is typical of L-PBF components, limits the list of available techniques, as does the component material.

Any component is designed and fabricated to serve a particular purpose during its service life. The service loads, mechanical and thermal fatigue, aging and others will determine the component material, geometry and the defects that need to be reliably detected during fabrication and later in service. In the modern fabrication environment, the design criteria and especially the allowable defect type, size, location and other characteristics are specified early at the design stage based on previous experience, dedicated research, laboratory and field trials. The detectable defect, or the defect that could be missed, will be constrained by the capabilities of available NDE techniques.

It is not very likely that parts with high level of geometric complexity and possible stress risers such as heat exchange features (e.g., fins, ribs), meshes and lattices will be exposed to excessive static and dynamic loads that will require detection and characterization of very small defects.

On the other hand, load critical parts will be designed with minimum stress risers if any, smooth surfaces and thicker sections that will require detection of small and tight, possibly planar surface breaking and slightly subsurface defects. Volumetric NDE techniques such as X-ray CT and PCRT, could be used for components with high level (Group 4 and 5) geometric complexity, multiple load paths and possibly larger allowable defects. NDE techniques such as RT, PAUT, AEC and PT, capable of detecting small surface and subsurface planar defects will be required where components with lower level of geometric complexity (Group 1 through 3) could be exposed to high level of static and dynamic loads, thermal cycling, corrosion and others.

Microstructure, stress and other types of characterization may have to be conducted along with defect detection during fabrication of critical components. Contact and non-contact ACPD, ECCS, EIT or ICT and similar techniques could be employed to characterize components with lower geometric complexity from Groups 1 to 3. These techniques can also be used to test dedicated spots or representative specimens from components with a higher level of geometric complexity such as Groups 4 and 5.

5.3 Down-selection of NDE Techniques

Table 5 shows a matrix of NDE techniques applied against the component complexity groupings. While most of the techniques are applicable to complexity Group 1 and 2, and some to Group 3, only PCRT and the X-ray CT techniques would be applicable to Group 4 and 5. Of these two methods, PCRT is a screening technique for parts like turbine blades and smaller. It could be used to determine bulk performance, not to classify a defect. The only current industrial NDE technique capable of inspecting Group 4 and 5 components is X-ray CT. The impact of process induced defects is minimal and as described, there are a few sources in the open literature that mention the use of X-ray CT to inspect nickel and titanium.

Table 5. Down-selection of NDE Technique for Different Complexity Categories

NDE Technique	Geometry Complexity Group					Comments
	1	**2**	**3**	**4**	**5**	
VT	Y	Y	P[(c)]	NA	NA	
LT	NA	NA	Y	Y	NA	Screening
PT	Y	Y	P[(a)]	NA	NA	
PCRT	Y	Y	Y	Y	Y	Screening; size restrictions (e.g., compressor blades)
EIT	Y	Y	NA	NA	NA	Screening; size restrictions
ACPD	Y	Y	P[(c)]	NA	NA	Isolated microstructure and/or stresses
ET	Y	Y	P[(c)]	NA	NA	
AEC	Y	Y	P[(c)]	NA	NA	
PAUT	Y	Y	P[(b)]	NA	NA	
UT	Y	Y	P[(b)]	NA	NA	
RT	Y	Y	P[(d)]	NA	NA	
X-Ray CT	Y	Y	Y	Y	NA	
X-ray Micro CT	Y	Y	Y	Y	Y	

Key:
    Y = Yes, technique applicable
    P = Possible to apply technique given correct conditions
    NA = Technique Not applicable

Notes:
    (a) Only surfaces providing good access for application and cleaning
    (b) Areas where shadowing of acoustic beam is not an issue
    (c) External surfaces and internal surfaces where access through conduits or guides can be provided
    (d) Areas where large number of exposures/shots are not required

5.4 Technical Gaps

There were a limited number of studies found in the open literature investigating NDE techniques for post process inspection of AM components. Due to the limited number and scope of available studies, performance of NDE techniques, even the most promising, cannot be reliably evaluated or anticipated when testing AM components. The challenge presented by the most complex AM parts (e.g., Group 4 and Group 5) has not been adequately addressed, even for existing subtractive technologies. The following three issues represent three significant technical gaps: 1) limited number of NDE studies for AM; 2) limited scope of NDE studies for AM; and, 3) the challenges of part complexity for existing subtractive technologies.

5.5 Methodology to Address Technical Gaps

Regardless of what NDE technique is selected to inspect an AM component, it must be qualified or quantified.[112-117] The qualification or quantification process is a systematic assessment of the NDE equipment, procedure and/or operators' capabilities to detect, characterize, and size certain

defects and conditions. There are different levels of qualification, quantification or NDE validation depending on industry, inspection objectives, criticality, and others.

One possible way to quantify the NDE process is to conduct a Technical Justification (TJ) and, if required, practical trials.[112] In general, the NDE equipment and procedures can be quantified through TJ and/or by open trials, while NDE operators will be quantified through TJ or blind trials. Typically, industry uses blind trials to quantify the entire NDE system (equipment, procedures, and operators).

At a minimum, the TJ would consist of three parts including an introduction with a description of the inspection and quantification objectives, NDE procedure and personnel certification, and training information. The TJ contents may be expanded to include an overview of the NDE procedure used in previous quantification efforts, a list of affected NDE essential parameters, predictions by computer modeling (model assisted probability of detection included) and experimental evidence from previous qualification or quantification activities.

The main outcome of the TJ review is a decision based on provided evidence on whether the proposed NDE system meets the inspection objectives expressed as probability of detection (POD) and other criteria such as accuracy of sizing, false call rate, discontinuity location accuracy, characterization, and resolution in terms of interacting discontinuity separation. A decision would also be made on the extent and type of practical trials (if needed) to support the expected or claimed NDE system performance in the TJ.

Results of NDE quantification/qualification will provide information about the ability of NDE equipment, procedure, or operator to meet the AM component inspection objectives. The information might contain POD, sizing accuracy statistics and other quantifiers for some or all of the three quantification components ─ equipment, procedures, and operators. In some cases, quantification may be accomplished by review of TJ documents from previous qualification or quantification trials. This option may not be available for AM components because results from such trials for AM components were not found in the open literature.

All contracting parties along with NDE vendors or providers are involved to determine the scope and performance level of the quantification process needed to meet the applicable inspection requirements or objectives. It is important to identify the NDE performance level early in the planning process so that adequate time and resources can be allotted. This process can take several months and requires good coordination between the different entities involved.

6.0 CONCLUSIONS

The following conclusions can be drawn from the literature review:

- L-PBF and EB-PBF are capable of producing complex parts made of titanium and nickel base alloys of interest to aerospace industry to meet near and far term objectives.

- Typical flaws for L-PBF and EB-PBF are pores, lack of fusion, cracking, delamination, and balling. Change of shape and dimensions, residual stresses, surface roughness and microstructure will also affect the NDE process and capabilities.

- Small flaw sizes in the range of beam size 50 to 100 µm pose additional challenges to any conventional and advanced NDE technique.

- AM component complexity was qualitatively divided into five groups with Group 4 and 5 being the most complex where traditional subtractive fabrication technologies would not be applicable. Group 4 and 5 are also expected to be the most difficult to inspect with NDE after fabrication.

- There were limited references to existing NDE techniques being used for examination of AM components and parts, indicating a significant technical gap.

- Based on preliminary analysis of NDE techniques, magnetic particle, microwave and terahertz inspection were not considered in this study due to the inability to detect flaws in electrically conductive and non-magnetic titanium and nickel-base alloys.

- X-ray computed tomography techniques may be applicable to geometries up to Group 5 complexity. It has potential to provide resolution in the range from 50 to 100 µm needed for AM defect detection and shape validation.

- Other techniques such as enhanced visual testing, process compensated resonance testing, flexible array eddy current and flexible array ultrasonics have potential to inspect components up to Group 3 complexity when coupled with advanced tools for data acquisition, processing and imaging.

- Specialized ultrasonic techniques based on acoustic attenuation and velocity measurements, and electromagnetic techniques capable of conductivity and/or magnetic permeability measurements and imaging have potential applications for microstructure and residual stress characterization of AM parts.

- In the long term, proven medical techniques such as X-ray through transmission, ultrasonic pulse-echo and through transmission tomography and emission tomography may be transferred and adapted to examine AM components after fabrication.

7.0 RECOMMENDATIONS

The recommendations are as follows:

- *Near-term*

  – Prepare a methodology and conduct a comprehensive study to evaluate X-ray computed tomography performance for highly complex geometry Group 4 and 5 parts that may involve: selection of AM component(s); identification of critical defects and conditions that need to be reliably detected and characterized; preparation of specimens with statistically significant number of representative AM defects and conditions; examination of specimens with selected X-ray CT system(s); sectioning of specimens for establishing NDE performance; and, evaluation of NDE performance and reporting of results.

  – Prepare a methodology and conduct a comprehensive study to evaluate performance of process compensated resonance testing as high speed screening technique for geometry complex parts Group 4 and 5.

  – Prepare a methodology and conduct a comprehensive study to evaluate performance of flexible array eddy current and flexible phased array ultrasonic techniques for components with complexity Group 1 through 3 requiring NDE examination for small surface and subsurface tight planar flaws.

  – For NDE monitoring and evaluation of microstructure, strain, anisotropy, hardness and residual stresses, investigate how these properties are correlated to electrical conductivity, magnetic permeability, acoustic velocity, acoustic attenuation and others.

- *Mid- and Far-Term*

  – Optimize further qualified advanced NDE techniques for complex geometries to reduce cost and increase speed of inspection.

  – Prepare or update codes, standards and specifications for NDE of AM components after fabrication.

  – Evaluate feasibility and transition emerging and advanced NDE technologies from medical (e.g., pulse-echo and through transmission ultrasonic tomography) or other industries, where applicable.

  – Evaluate performance of emerging and advanced NDE techniques for examination of flight critical AM components.

8.0 REFERENCES

[1] Bourell, D. L., Beaman, J. B., Leu, M. C., & Rosen, D. W., A brief history of additive manufacturing and the 2009 roadmap for additive manufacturing: looking back and looking ahead. In US-Turkey Workshop on Rapid Technologies, 2009

[2] Milberg, Joachim, and M. Sigl. "Electron beam sintering of metal powder." Production Engineering 2, no. 2 (2008): 117-122.

[3]   Gibson, Ian, David W. Rosen, and Brent Stucker. Additive manufacturing technologies. New York: Springer, 2010.

[4]   Chui, Michael, Jacques Bughin, Richard Dobbs, Peter Bisson, and Alex Marrs. Disruptive technologies: Advances that will transform life, business, and the global economy. Vol. 180. San Francisco, CA: McKinsey Global Institute, 2013.

[5]   Wohlers, Terry T. Wohlers Report 2014: Additive Manufacturing and 3D Printing State of the Industry: Annual Worldwide Progress Report. 2014.

[6]   Slattery, K, B. Slaughter, E. Speore, J. Good, S. Gilley and C. McLemore,"Evaluation of ARCAM Deposited Ti-6Al-4V", 2nd SAlAS Symposium, pp. 14-16 September 2008, Stellenbosch, South Africa.

[7]   Wong, Kaufui V., and Aldo Hernandez. "A review of additive manufacturing." ISRN Mechanical Engineering 2012 (2012).

[8]   Guo, Nannan, and Ming C. Leu. "Additive manufacturing: technology, applications and research needs." Frontiers of Mechanical Engineering 8, no. 3 (2013): 215-243.

[9]   ASTM, F2792 – 12a, Standard Terminology for Additive Manufacturing Technologies. (2012).

[10]   Bineli, Aulus Roberto Romão, Ana Paula Gimenez Peres, André Luiz Jardini, and Rubens Maciel Filho. "Direct metal laser sintering (DMLS): Technology for design and construction of microreactors." In 6º CONGRESS OBRASILEIRO DE ENGENHARIA DE FABRICA ÇÃO, vol. 11. 2011.

[11]   Jamshidinia, Mahdi, Fanrong Kong, and Radovan Kovacevic. "Numerical Modeling of Heat Distribution in the Electron Beam Melting® of Ti-6Al-4V." Journal of Manufacturing Science and Engineering 135, no. 6 (2013): 061010

[12]   Mahale, Tushar Ramkrishna, (2009), "Electron Beam Melting of Advanced Materials and Structures", PhD Dissertation, North Carolina State University, Raleigh.

[13]   http://www.iwb.tum.de/en/Equipment_Manufacturing-p-23685392.html

[14]   Gong, Xibing, Ted Anderson, and Kevin Chou. "Review on powder-based electron beam additive manufacturing technology." In *ASME/ISCIE 2012 International Symposium on Flexible Automation*, pp. 507-515. American Society of Mechanical Engineers, 2012.

[15]   Facchini, Luca, Emanuele Magalini, Pierfrancesco Robotti, and Alberto Molinari. "Microstructure and mechanical properties of Ti-6Al-4V produced by electron beam melting of pre-alloyed powders." *Rapid Prototyping Journal* 15, no. 3 (2009): 171-178.

[16]   http://cordis.europa.eu/result/rcn/62346_en.html)

[17]   Biemond, J. E., G. Hannink, N. Verdonschot, and P. Buma. "Bone ingrowth potential of electron beam and selective laser melting produced trabecular-like implant surfaces with and without a biomimetic coating." *Journal of Materials Science: Materials in Medicine* 24, no. 3 (2013): 745-753.

[18]   http://www.arcam.com/wp-content/uploads/Arcam-Ti6Al4V-Titanium-Alloy.pdf

[19]   Murr, L. E., E. V. Esquivel, S. A. Quinones, S. M. Gaytan, M. I. Lopez, E. Y. Martinez, F. Medina et al. "Microstructures and mechanical properties of electron beam-rapid

manufactured Ti–6Al–4V biomedical prototypes compared to wrought Ti–6Al–4V." *Materials Characterization* 60, no. 2 (2009): 96-105.

[20]   Eschey, C., S. Lutzmann, and M. F. Zaeh. "Examination of the powder spreading effect in Electron Beam Melting (EBM)." *Solid Freeform Fabrication, Austin, TX, August* (2009): 3-5.

[21]   Koike, M., Preston Greer, Kelly Owen, Guo Lilly, Lawrence E. Murr, Sara M. Gaytan, Edwin Martinez, and Toru Okabe. "Evaluation of titanium alloys fabricated using rapid prototyping technologies—Electron beam melting and laser beam melting." *Materials* 4, no. 10 (2011): 1776-1792.

[22]   Bourell, David L., Ming C. Leu, and David W. Rosen. "Roadmap for additive manufacturing: identifying the future of freeform processing." The University of Texas, Austin (2009).

[23]   Huang, Yong, and Ming C. Leu. "Frontiers of Additive Manufacturing Research and Education." (2014).

[24]   Antonysamy, Alphons Anandaraj. "Microstructure, texture and mechanical property evolution during additive manufacturing of Ti6Al4V alloy for aerospace applications." (2012-A).

[25]   Attar, Elham. "Simulation of selective electron beam melting processes." PhD diss., Ph. D. Thesis, 2011.

[26]   Gong, Haijun, Khalid Rafi, Thomas Starr, and Brent Stucker. "The Effects of Processing Parameters on Defect Regularity in Ti-6Al-4V Parts Fabricated By Selective Laser Melting and Electron Beam Melting., In Proceeding of the Twenty Forth Annual International Solid Freeform Fabrication Symposium, August, 2013, pp. 424-439.

[27]   Gaytan, S. M., Murr, L. E., Medina, F., Martinez, E., Lopez, M. I., and Wicker,R. B., 2009, "Advanced Metal Powder Based Manufacturing of Complex Componentsby Electron Beam Melting," Mater. Technol., 24(3), pp. 181–190.

[28]   Vrancken, B., R. Wauthle, J. P. Kruth, and J. Van Humbeeck. "Study of the influence of material properties on residual stress in selective laser melting", In Proceeding of the Twenty Forth Annual International Solid Freeform Fabrication Symposium, August, 2013, pp. 393-407.

[29]   Zaeh, Michael F., and Gregor Branner. "Investigations on residual stresses and deformations in selective laser melting." Production Engineering 4, no. 1 (2010): 35-45.

[30]   Li, Ruidi, Jinhui Liu, Yusheng Shi, Li Wang, and Wei Jiang. "Balling behavior of stainless steel and nickel powder during selective laser melting process." The International Journal of Advanced Manufacturing Technology 59, no. 9-12 (2012): 1025-1035.

[31]   Gu, Dongdong, and Yifu Shen. "Balling phenomena in direct laser sintering of stainless steel powder: metallurgical mechanisms and control methods." Materials & Design 30, no. 8 (2009): 2903-2910

[32]   Safdar, Adnan, H. Z. He, Liu-Ying Wei, A. Snis, and Luis E. Chavez de Paz. "Effect of process parameters settings and thickness on surface roughness of EBM produced Ti-6Al-4V." Rapid Prototyping Journal 18, no. 5 (2012): 401-408.

[33] Jamshidinia, Mahdi, and Radovan Kovacevic. "The influence of heat accumulation on the surface roughness in additive manufacturing by electron beam melting (EBM)®.", 2014 ASPE Spring Topical Meeting, Dimensional Accuracy and Surface Finish in Additive Manufacturing, Apr. 13-16, 2014, Berkeley, CA, USA

[34] S. Das. Physical aspects of process control in selective laser sintering of metals. Advanced Engineering Materials, 5: 701-711, 2003.

[35] M. Agarwala, D. Bourell, J. Beaman, H. Marcus, and J. Barlow. Direct selective laser sintering of metals. Rapid Prototyping Journal, 1 : 26-36, 1995.

[36] Campanelli, Sabina L., Nicola Contuzzi, Antonio D. Ludovico, Fabrizia Caiazzo, Francesco Cardaropoli, and Vincenzo Sergi. "Manufacturing and Characterization of Ti6Al4V Lattice Components Manufactured by Selective Laser Melting." Materials 7, no. 6 (2014): 4803-4822.

[37] Ponader, Sabine, Eleftherios Vairaktaris, Peter Heinl, Cornelius V. Wilmowsky, Andreas Rottmair, Carolin Körner, Robert F. Singer et al. "Effects of topographical surface modifications of electron beam melted Ti-6Al-4V titanium on human fetal osteoblasts." Journal of biomedical materials research Part A 84, no. 4 (2008): 1111-1119.

[38] O. Kerbrat, P. Mognol, J.Y. Hascoet, "Manufacturing Complexity Evaluation for Additive and Subtractive Processes: Application to Hybrid Modular Tooling", IRCCyN (Institut de Recherche en Communications et Cybernétique de Nantes), MO2P Team1 rue de la Noë, BP 92101, 44321, Nantes Cedex 03, France., pp 519-530, September 10, 2008

[39] Kroll, J., Botta, S., Breuninger, A., "Adaptive Quality Assurance of the Product Development Process of Additive Manufacturing with Modern 3D Data Evaluation Methods", *Fraunhofer Institut für Produktionstechnik und Automatisierung, Nobelstraße 12, 70569 Stuttgart, Germany*, pp 1-11 , 2013

[40] General Electric Company, "Jet Engine Bracket from Indonesia Wins 3D Printing Challenge", http://www.gereports.com/post/77131235083/jet-engine-bracket-from-indonesia-wins-3d-printing. Accessed August 20, 2014.

[41] EOS, "Tooling: Additive Manufacturing Permits Optimized Cooling for Maximum Production Efficiency," http://www.eos.info/press/customer_case_studies/salcomp, accessed August 20, 2014.

[42] Within-Lab, "Case Study: Heat Exchanger", http://www.within-lab.com/case-studies/index11.php, Accessed August 20, 2014.

[43] Visual Inspection, Nondestructive Evaluation and Quality Control, Vol 17, Metals Handbook, 9-th Edition, pp. 3-11, ASM International, Metals Park, OH, 1989.

[44] Forsyth, D. S., J. P. Komorowski, and R. W. Gould, A. Marincak, "Automation of Enhanced Visual NDT Techniques", PACNDT '98 - Proceedings, 1st Pan American Conference for Nondestructive Testing, Toronto, 14-18 September 1998.

[45] Leak Testing, Nondestructive Evaluation and Quality Control, Vol 17, Metals Handbook, 9-th Edition, pp. 57-70, ASM International, Metals Park, OH, 1989.

[46] FAA Center for Aviation Systems Reliability, "Engineering Assessment of Fluorescent Penetrant Inspection," 2002,**http://www.cnde.iastate.edu/faa-casr/fpi/Public.htm**. Accessed on August 06, 2014.

[47] DOT/FAA/AR-01/95, "Study of the Factors Affecting the Sensitivity of Liquid Penetrant Inspections: Review of Literature Published from 1970 to 1998", US Department of Transportation, Federal Aviation Administration, Office of Aviation Research, Washington, D.C. 20591, January 2002.

[48] ASTM E1209 – 10, "Fluorescent Liquid Penetrant Testing Using the Water-Washable Process".

[49] ASTM E2534 – 10, "Standard Practice for Process Compensated Resonance Testing via Swept Sine Input for Metallic and Non-Metallic Parts".

[50] Schwarz, J, J. Saxton, and L. Jauriqui, "Process Compensated Resonant Testing in Manufacturing Process Control", *Materials Evaluation*, Vol. 63, No. 7, pp. 736-739, July 2005.

[51] Piotrowski D., L. Hunter, G. Weaver, L. Jauriqui, E. Biedermann, G. Gatewood, "Update of Process Compensated Resonance Testing (PCRT) Programs at Delta TechOps", *56th Annual A4A NDT Forum*, September 23-27, 2013. Indianapolis, Indiana.

[52] Boillat, E., Fivat, D., Jhabvala, J., Matthey, M., and Glardon, R., "A Review of Different Techniques to Characterize the Mechanical Properties of SLS Parts - Focus on Resistivity Measurements", *Innovative Developments in Virtual and Physical Prototyping - Proceedings of the 5th International Conference on Advanced Research and Rapid prototyping*, September 28, 2011 - October 1, 2011, Taylor and Francis Inc., pp 281-286, 2012.

[53] Bogdanov, G., J. Wiggins, K. Bertagnolli, and R. Ludwig, "An Electrical Conductivity Inspection Methodology of Polycrystalline Diamond Cutters," *Review of Progress in Quantitative Nondestructive Evaluation*, Vol. 32, edited by D. O. Thompson and D. E. Chimenti, Denver, Colorado, pp. 457-464, July 15-20, 2012.

[54] Bogdanov, G., J. Wiggins, J. Rhodes, K. Bertagnolli, and R. Ludwig, "Instrumentation Development for Electrical Conductivity Imaging in Polycrystalline Diamond Cutters," *Review of Progress in Quantitative Nondestructive Evaluation*, Vol. 33, edited by D. O. Thompson and D. E. Chimenti, Baltimore, Maryland, pp. 1623-1630, July 21-26, 2013.

[55] Madhi, E., and P. B. Nagy, "In-situ Resistivity Monitoring of Microstructure Evolution in IN718 Nickel-base Superalloy", *Review of Progress in Quantitative Nondestructive Evaluation*, Vol. 28, edited by D. O. Thompson and D. E. Chimenti, Chicago, Illinois, pp. 1209-1215, July 20-25, 2008.

[56] Madhi, E., and P. B. Nagy, "On the Influence of Cold Work on Resistivity Variations with Thermal Exposure in IN-718 Nickel-base Superalloy", *Review of Progress in Quantitative Nondestructive Evaluation*, Vol. 29, edited by D. O. Thompson and D. E. Chimenti, Kingston, Rhode Island, pp. 1325-1332, July 26-31, 2009.

[57] Prajapati, S., P. B. Nagy, and R. Cawley, "Potential Drop Detection of Creep Damage in the Vicinity of Welds", *Review of Progress in Quantitative Nondestructive Evaluation*,

Distribution Statement A: Approved for public release; distribution unlimited.

Vol. 31, edited by D. O. Thompson and D. E. Chimenti, Burlington, Vermont, , pp. 417-424, July 17 – 22, 2011.

[58] Sekine, Y., and H. Soyama, "Evaluation of Equibiaxial Compressive Stress Introduced into Austenitic Stainless Steel Using an Eddy Current Method", *Journal of Nondestructive Evaluation*, Vol. 31, No. 2, June 2012, pp. 99-107.

[59] Shen, Y., C. C. H. Lo, N. Nakagawa, and A. M. Frishman, "Residual Stress Profile Assessment by Eddy Current for Shot Peened Nickel Superalloy", *Journal of Nondestructive Evaluation*, Vol. 29, No. 1, March 2010, pp. 1-13.

[60] Hillmann, S., H. Heuer, H.-U. Baron, J. Bamberg, A. Yashan, and N. Meyendorf, "Near-surface Residual Stress Profiling with High Frequency Eddy Current Conductivity Measurement", *Review of Progress in Quantitative Nondestructive Evaluation*, Vol. 28, edited by D. O. Thompson and D. E. Chimenti, Chicago, Illinois, pp. 1349-1355, July 20-25, 2008.

[61] Hillmann, S., H. Heuer, A. Robbert, H.-U. Baron, J. Bamberg, and N. Meyendorf, "Experimental-based Discussion for the Separation of Residual Stresses and Cold Work in Shot Peened IN718 Using High Frequency Eddy Current Spectroscopy", *Review of Progress in Quantitative Nondestructive Evaluation*, Vol. 29, edited by D. O. Thompson and D. E. Chimenti, Kingston, Rhode Island, pp. 1349-1356, July 26-31, 2009.

[62] Todorov, E. I., "Feasibility of Detection of Air Contamination in Reactive Alloy Welds with Eddy Current Methods", *International Chemical and Petroleum Industry Inspection Technology (ICPIIT) X Conference*, Houston, Texas, pp. 105-112, June 20-23, 2007

[63] Todorov, E., Mohr, W., and Lozev, M., "Detection and Sizing of Fatigue Cracks in Steel Welds with Advanced Eddy Current Techniques," *Review of Progress in Quantitative Nondestructive Evaluation, Vol. 27*, edited by D. O. Thompson and D. E. Chimenti, Golden, Colorado, pp. 1058-1065, July 22-27, 2007.

[64] Lafontaine, G. and Samson, R., "Eddy Current Array Probes for Faster, Better and Cheaper Inspections", *2nd International Conference on NDE in Relation to Structural Integrity for Nuclear and Pressurized Components*, New Orleans May 2000.

[65] Todorov, E. and W. Mohr, "Advanced Eddy Current Inspection of Steel Structures", EWI Project No. 49850GTO, EWI, July 05, 2007.

[66] Decitre, J.-M., D. Premel, G. Mangenet, E. Juliac, and W. D. Feist, "Flexible EC Array Probe for the Inspection of Complex Parts Developed within the European VERDICT Project", *European Conference of Non-Destructive Testing 2006*, Berlin, September 25-29.

[67] Goldfine, N., V. Zilberstein, J. C. Cargill, D. Schlicker, I. Shay, A. Washabaugh, V. Tsukernik, D. Grundy, and M. Windoloski, "MWM-Array Eddy Current Sensors for Detection of Cracks in Regions with Fretting Damage", *Materials Evaluation*, Vol 60, No. 7, July 2002.

[68] Endo, H., A. Nishimizo, M. Tooma, H. Ouchi, I. Yoshida, Y. Nonaka, and K. Otani, "Signal Evaluation System of Flexible Array ECT Probes for Inspecting Compexly Shaped Surfaces", *Review of Progress in Quantitative Nondestructive Evaluation*, Vol. 30,

edited by D. O. Thompson and D. E. Chimenti, San Diego, California, pp. 597-603, July 18-23, 2010.

[69] Introduction to Phased Array Ultrasonic Technology Applications, R/D Tech Guidelines. R/D Tech Inc., 2004.

[70] Hopkins, D., G. Neau, and L. Le Ber, "Ultrasonic Phased Array. Advanced Phased Array Measurement and Imaging Techniques", International Workshop, Smart Materials, Structures & NDT in Aerospace Conference, NDT in Canada, 2-4 November 2011, Montreal, Quebec, Canada.

[71] Casula, O., Toullelan, G., Roy, O. and Dumas, Ph, "Ultrasonic Nondestructive Testing of Complex Components with Flexible Phased-Array Transducers", *10th European Conference on Non-Destructive Testing*, Moscow 2010, June 7-11.

[72] Spencer, R., Porter, N., Lozev, M., Todorov, E., Reverdy, F., Benoist, P., and Dumas, P. "Enhanced Defect Detection and Sizing Accuracy Using Matrix Phased Array Ultrasonic Tools", *Rio Pipeline Conference and Exposition 2009*, Rio de Janeiro, Brazil, September, 22-24, 2009.

[73] Spencer, R., Todorov, E., White, P., Porter, N., and Lozev, M., "Enhanced Defect Detection and Sizing Accuracy Using Matrix Phased Array Ultrasonic Tools", DTPH56-08-T-000002, *U.S. Department of Transportation Pipeline and Hazardous Materials Safety Administration*, Office of Pipeline Safety, Washington, DC, 2011.

[74] Jeong, H., "Focusing a Flexible Ultrasonic Array Transducer Using a Time reversal Technique for Discontinuities within Complex Geometries", *Materials Evaluation,* pp. 173-179, Vol. 70, No. 2, February 2012.

[75] Jeong, H., "Time Reversal-based Beam Focusing of an Ultrasonic Phased Array Transducer on a Target in Anisotropic and Inhomogeneous Welds", *Materials Evaluation,* pp. 589-596, Vol. 72, No. 5, May 2014.

[76] Bewlay, B. P., Deaton Jr, J. B., Gigliotti, M. F. X., Gilmore, R. S., Salishchev, G. A., "Method for producing homogeneous fine grain titanium alloys suitable for ultrasonic inspection", EP 1433863 A1, 2004

[77] Nicoletti, Denise, Nihat Bilgutay, and Banu Onaral. "Power-law relationships between the dependence of ultrasonic attenuation on wavelength and the grain size distribution." The Journal of the Acoustical Society of America 91, no. 6 (1992): 3278-3284.

[78] Gorman, M. D., Woodfield, A. P., "Processing of titanium-alloy billet for improved ultrasonic inspectability", EP 1136582 A1, 2001.

[79] Telschow, K.L., "Noncontacting NDE for Materials Characterization", Idaho National Engineering Laboratory, 1995.

[80] Karthik, N. V., Hengfeng Gu, Deepankar Pal, Thomas Starr, and Brent Stucker. "High Frequency Ultrasonic Non Destructive Evaluation of Additively Manufactured Components.", In Proceeding of the Twenty Forth Annual International Solid Freeform Fabrication Symposium, August, 2013, pp. 311-325.

[81] Paxson, A. J., Shamblen, C. E., "Homogenizing and forming ingot, thermochemically treating billet to recrystallize, cooling, heating, forging", US 5277718 A, 1994.

[82] http://www.teledynedalsa.com/imaging/knowledge-center/appnotes/ccd-vs-cmos/

[83] Gong, Xibing, Ted Anderson, and Kevin Chou. "Review on powder-based electron beam additive manufacturing technology." In *ASME/ISCIE 2012 International Symposium on Flexible Automation*, pp. 507-515. American Society of Mechanical Engineers, 2012.

[84] CT artifacts: Causes and reduction techniques", F Edward Boas & Dominik Fleischmann* Department of Radiology, Stanford University School of Medicine, 300 Pasteur Drive, Stanford, CA 94305, USA

[85] "Fundamentals of Microfocus Radiography", Feinfocus Rontgen-Systeme GmbH, Im Bahlbrink, P.O.Box 12 2, D-30812 Garbsen, German.

[86] http://www.ndeed.org/EducationResources/CommunityCollege/Radiography/Physics/Geo metricUnsharp.htm

[87] ASTM, 1992. Standard Guide for Computed Tomography (CT) Imaging, ASTM Designation E 1441 - 92a. In: 1992 Annual Book of ASTM Standards, Section 3 Metals Test Methods and Analytical Procedures. ASTM, Philadelphia, pp. 690-713

[88] METALJET - Liquid Metal Jet X-ray source for Structural Biology An X-Ray Revolution Without Rotation", Bruker Corperation Product Sheet SC-XRD 49, Bruker AXS Inc. .

[89] "Very Large Area CMOS Active-Pixel Sensor for Digital Radiography", Michael Farrier, Thorsten Graeve Achterkirchen,Gene P. Weckler, Alex Mrozack, IEEE TRANSACTIONS ON ELECTRON DEVICES, VOL. 56, NO. 11, NOVEMBER 2009.

[90] "Selenium coated CMOS passive pixel array for medical imaging", Shaikh Hasibul Majid, Amir H. Goldan, Bahman Hadji, George Belev, Safa Kasap, Karim S. Karim, SPIE Vol. 7961 79614L-10

[91] Herman, G, "Fundamental of Computerized Tomography" Springer-Verlag London Limited 2009, p 11.,37(PDF#)

[92] "Iterative Reconstruction for Transmission Tomography on GPU Using Nvidia CUDA", Damien Vintache, Bernard Humbert, David Brasse, TSINGHUA SCIENCE AND TECHNOLOGY, ISSNl l1007-0214l l02/20l lpp11-16,Volume 15, Number 1, February 2010.

[93] "Practical cone-beam algorithm", L. A. Feldkamp, L. C. Davis, and J. W. Kress, Journal of the Optical Society of America A, 1984, 1(6): 612-619.

[94] "Principles of Computerized Tomographic Imaging", A C Kak, M Slanet., New York: IEEE Press, 1988

[95] "Advantages of CT in 3D Scanning of Industrial Parts", Julien Noel, ©2008 3D Scanning Technologies Magazine, December 2008

[96] "Distributed and hardware accelerated computing for clinical medical imaging using proton computed tomography (pCT)", Nicholas T. Karonis, Kirk L. Duffin, Caesar E. Ordoñeza, Bela Erdelyi,Thomas D. Uramc, Eric C. Olson, George Coutrakon, Michael E. Papka, Journal of Parallel and Distributed Computing, Vol 73, 2013.

[97] De Chiffre, L., Carmignato, S., Kruth, J-P., Schmitt, R. and Weckenmann, A. "Industrial applications of computed tomography." CIRP Annals-Manufacturing Technology **63**(2) 2014, pp. 655–77.

[98] Kruth, J-P., Bartscher, M.P., Carmignato,S. Schmitt, R., De Chiffre, L. and Weckenmann, A. "Computed tomography for dimensional metrology." CIRP Annals-Manufacturing Technology 60(2) 2011, pp. 821-42.

[99] Bossi, R. H., Cline, J.H., Georgeson, G.E., "X-Ray Computed Tomographic Inspection of Castings", Review of Progress in Quantitative Nondestructive Evaluation, 1991, pp. 1783-1790.

[100] G.E, Bossi, Georgeson, R.H. and Rempt, R.D. "X-Ray Computed Tomography for Emerging Aerospace Materials and Processes Development," AFRL Report WL-TR-93-4054, May 1, 1993.

[101] Georgeson, G.E, Bossi, R.H. and Rempt, R.D. "X-Ray Computed Tomography for Casting Demonstration," AFRL Report WL-TR-93-4048, May 1, 1993.

[102] Bossi, R.H. and Nelson, J. M. "X-Ray Computed Tomography Standards," AFRL Report WL-TR-43-4021, February, 1994.

[103] Neira Arce, Alderson. Thermal Modeling and Simulation of Electron Beam Melting for Rapid Prototyping on Ti6Al4V Alloys. 2012.

[104] Leuders, S., M. Thöne, A. Riemer, T. Niendorf, T. Tröster, H. A. Richard, and H. J. Maier. "On the mechanical behaviour of titanium alloy TiAl6V4 manufactured by selective laser melting: Fatigue resistance and crack growth performance." International Journal of Fatigue 48 (2013): 300-307.

[105] Radovan, H., Zivcak, J., Toth, T. Majernik, J., and Lisy, M. "Evaluation of custom-made implants using industrial computed tomography." In Digital Technologies (DT), 2014 10th International Conference on, pp. 82-86. IEEE, 2014.

[106] Kim, B., Yue, S., Zhang, Z., Jones, E., Jones, J., Lee, P., "Additive Manufactured Porous Titanium Structures: Through-Process Quantification of Pore and Strut Networks"; Journal of Materials Processing Technology, 214 (2014) 2706-2715

[107] http://www.mayoclinic.org/tests-procedures/spect-scan/basics/definition/prc-20020674

[108] http://www.nlm.nih.gov/medlineplus/ency/article/003827.htm

[109] Morollon, C., Be, M. M., Chechev, V., and Egorov, A., "CEA Table de Radionucleides - Technetium-99m", LNHB-KRI, 5/2012.

[110] http://www.rapidrecoveryhyperbarics.com/sCaN%20aFtEr2.jpg

[111] Seo, H., Lee, S. H., Jeong, J. H., Kim, C. H., Lee, C.S, and Lee, J. S., "Feasibility Study on Hybrid Medical Imaging Device Based on Compton Imaging and Magnetic Resonance Imaging", ElsevierLtd. Applied Radiation and Isotopes 67 (2009) 1412–1415.

[112] Todorov, E., R. Spencer, and M. Lozev, "Methodologies for Automated Ultrasonic Testing Performance Quantification", *Materials Evaluation,* Vol. 72, No. 6, pp. 812-824, June 2014.

[113] ASME Boiler & Pressure Vessel Code (BPVC), Section V, "Article 14 – Examination System Qualification," *ASME,* July 1, 2013.

[114] ENIQ, "European Methodology for Qualification of Non-destructive Testing, Issue 3, Report No. 31," *EUR EN 22906*, August 2007.

[115] MIL-HDBK-1823 (2009), "Nondestructive Evaluation System Reliability Assessment," *Department of Defense Handbook*.

[116] DNV-RP-F118, "Recommended Practice. Pipe Girth Weld AUT System Qualification and Project Specific Procedure Validation," *Det Norske Veritas*, October 2010.

[117] Nordtest Report, *NT TECHN REPORT 394*, Approved 1998-04.

9.0 LIST OF SYMBOLS, ABBREVIATIONS AND ACRONYMS

2D	Two Dimensional
3D	Three Dimensional
3D Printing	Three-dimensional Printing
AC	Alternate Current
ACPD	Alternate Current Potential Drop
AEC	Array Eddy Current
AM	Additive Manufacturing
a-Si TFT	Amorphous Silicon Thin-film Transistor
CAD	Computer-aided Design
CCD	Charged Couple Device
CMOS	Complementary Metal Oxide Semiconductor
CNC	Computer Numeric Control
CT	Computed Tomography
DACPD	Directional ACPD
DC	Direct Current
EB-PBF	Electron Beam Powder Bed Fusion
EC	Eddy Current
ECCS	Eddy Current Conductivity Spectroscopy
EIT	Electrical Impedance Tomography
ET	Eddy Current Testing
FCC	Face-centered Structure
GE	General Electric
HIP	Hot Isostatic Pressing
ICT	Impedance Computed Tomography
LPA	Linear Phased Array
L-PBF	Laser-Powder Bed Fusion
LT	Leak Testing
MDT	Metal Deletion Technique
ML-EM	Maximum Likelihood-Expectation Maximization
MPA	Matrix Phased Array

MT	Magnetic Particle Testing
NDE	Nondestructive Evaluation
OSC	Ordered Subsets Convex Algorithm
PAUT	Phased Array Ultrasonic Testing
PBF	Powder Bed Fusion
PCRT	Process Compensated Resonance Testing
PDC	Polycrystalline Diamond Cutters
PET	Positron Emission Tomography
POD	Probability of Detection
PT	Liquid Penetrant Testing
RT	Radiographic Testing
SEM	Scanning Electron Microscope
SIRT	Simultaneous Iterative Reconstruction Technique
SPECT	Single-Photon Emission Computed Tomography
STL	Stereo Lithography
TJ	Technical Justification
UT	Ultrasonic Testing
UTT	Ultrasound Transmission Tomography
VT	Visual Testing
X-ray CT	X-ray Computed Tomography
X-ray Micro FCT	X-ray Micro-focus Computed Tomography